Acta Pharmaceutica Sinica B 2024;14(10):4509–4525

Chinese Pharmaceutical Association
Institute of Materia Medica, Chinese Academy of Medical Sciences

Acta Pharmaceutica Sinica B

www.elsevier.com/locate/apsb
www.sciencedirect.com

ORIGINAL ARTICLE

Cocrystal@protein-anchoring nanococktail for combinatorially treating multidrug-resistant cancer

Jiahui Zou[a,†], Xuyang Xing[a,†], Chao Teng[a], Qingling Zhao[b], Wei He[a,*], Xuri Wu[c,*], Yuanzheng Xia[d,*]

[a]*School of Pharmacy, China Pharmaceutical University, Nanjing 211198, China*
[b]*School of Computer Science and Engineering, Nanjing University of Science and Technology, Nanjing 210094, China*
[c]*School of Life Science and Technology, China Pharmaceutical University, Nanjing 211198, China*
[d]*State Key Laboratory of Natural Medicines and Jiangsu Key Laboratory of Bioactive Natural Product Research, School of Traditional Chinese Pharmacy, China Pharmaceutical University, Nanjing 211198, China*

Received 15 April 2024; received in revised form 17 June 2024; accepted 10 July 2024

KEY WORDS

Cocktail;
Multidrug-resistant;
Co-delivery combined therapy;
Cytochrome C;
Nanocrystals

Abstract Multidrug resistance (MDR), the major mechanism by which various cancers develop specific resistance to therapeutic agents, has set up enormous obstacles to many forms of tumor chemotherapy. Traditional cocktail therapy administration, based on the combination of multiple drugs for anti-MDR chemotherapy, often suffers from inconsistent *in vivo* pharmacokinetic behaviors that cannot act synchronously on the lesions, leading to limited pharmacodynamic outcomes. Despite the emergence of nanomedicines, which has improved chemotherapeutic drugs' bioavailability and therapeutic effect on clinical application, these monotherapy-based nano-formulations still show poor progression in overcoming MDR. Herein, a "one stone and three birds" nanococktail integrated by a cocrystal@protein-anchoring strategy was purposed for triple-payload delivery, which paclitaxel-disulfiram cocrystal-like nanorods (NRs) were anchored with the basic protein drug Cytochrome *c* (Cyt C), followed by hyaluronic-acid modification. In particular, NRs were utilized as carrier-like particles to synchronously deliver biomacromolecule Cyt C into tumor cells and then promote cell apoptosis. Of note, on A549/Taxol drug-resistant tumor-bearing mice, the system with extraordinarily high encapsulation efficiency demonstrated prolonged *in vivo* circulation and increased tumor-targeting accumulation, significantly reversing tumor drug resistance and improving therapeutic efficacy. Our mechanistic study indicated that the

*Corresponding authors.
E-mail addresses: weihe@cpu.edu.cn (Wei He), xuriwu@cpu.edu.cn (Xuri Wu), xiayz@cpu.edu.cn (Yuanzheng Xia).
†These authors made equal contributions to this work.
Peer review under the responsibility of Chinese Pharmaceutical Association and Institute of Materia Medica, Chinese Academy of Medical Sciences.

https://doi.org/10.1016/j.apsb.2024.08.014

system induced the apoptosis of Taxol-resistant tumor cells through the signal axis P-glycoprotein/Cyt C/caspase 3. Collectively, this nanococktail strategy offers a promising approach to improve the sensitivity of tumor cells to chemotherapeutic drugs and strengthen intractable drug-resistant oncotherapy.

1. Introduction

Lung cancer is one of the cancers with the highest morbidity and mortality worldwide[1]. Among them, non-small cell lung cancer (NSCLC) is a kind of aggressive cancer that accounts for about 85% of increasing new cases year by year, and the 5-year survival rate of patients is barely 15%[2]. Chemotherapy is still the mainstream treatment for lung cancer[3]. However, the repeated/multiple use of chemotherapeutic drugs can lead to the generation of multidrug resistance (MDR) phenomenon in tumor cells, thus reducing the therapeutic effect and resulting in the failure of clinical chemotherapy[4]. The formation of MDR is a multifunctional and complicated progress[5,6], mainly including (i) reduced influx and increased efflux of chemotherapeutics by overexpressed membrane transporter protein-ATP-binding cassette (ABC); (ii) drug-resistant tumor cells can sequester drugs into vesicles and further excrete them through exocytosis; (iii) overexpressed of multiple metabolic enzymes inactivate drugs thereby erasing their anti-tumor effects; (iv) mutations of the surface receptors hinder the recognition of drug molecules and corresponding targets; (v) increased DNA repair enzyme activity of drug-resistant tumor cells can effectively inhibit drugs-induced DNA damage; (vi) suppressed ability of drugs to induce cell apoptosis by upregulated anti-apoptotic factors (*i.e.*, nuclear transcription factor-κB, B cell lymphoma-2, etc.); etc. As a result, overcoming MDR is a great challenge to treat drug-resistant tumors, urgently requiring new routines to improve therapeutic effects and obtain better clinical outcomes.

Most clinical chemotherapy failures stem from drug efflux by drug-resistant tumor cells and the overexpressed membrane transporter protein ABCs[7]. Among them, P-glycoprotein (P-gp), one of the ABCs involved in the formation of MDR, could mediate MDR by pumping out some intracellular substances as well as small molecule anticancer drugs (*e.g.*, paclitaxel and doxorubicin) *via* the energy generated by ATP hydrolysis[8]. Although the clinical chemotherapeutic nanomedicines (*e.g.*, paclitaxel albumin nanoparticles, doxorubicin liposomes, etc.) have been extensively used to improve the bioavailability and therapeutic efficacy of chemotherapeutic drugs to some extent, these single-drug nano-preparations are unable to treat multidrug-resistant tumors effectively. Hence, increasing studies have evidenced that the combination of P-gp inhibitors and anticancer drugs is promising to reduce the MDR-1 expression and regress tumor drug resistance, improving sensitivity of tumor cells to chemotherapeutic drugs and therapeutic effect.

Paclitaxel (PTX) is a chemotherapeutic agent approved by the US Food and Drug Administration (FDA) for treating various cancers[9]. Disulfiram (DSF) is a hydrophobic small molecule drug frequently used as an anti-alcoholic medicine. Recent findings suggest that DSF exhibits the potential to function as a P-gp inhibitor, which can reverse MDR by interacting with the P-gp binding site, thereby inhibiting the efflux pump activity of drug-resistant tumor cells and reducing the elimination of chemotherapeutic agents from tumor cells[10]. The combination of PTX and DSF is promising to sensitize tumor cells to PTX and kill drug-resistant lung tumor cells more effectively than alone[11]. In addition to conventional small molecule drugs, biomacromolecule drugs (*e.g.*, monoclonal antibodies, peptides, gene drugs, active proteins, etc.) as a unique anti-tumor pathway, play a significant role in tumor therapy due to high biocompatibility, low immunogenicity, and high targeting efficiency[12]. Cytochrome C (Cyt C) is an intracellular protein with an essential function in apoptosis, promoting apoptosis upon receiving damage to cellular mitochondria. However, Cyt C is often downregulated in cancer cells[13]. Therefore, based on triple-dimensional anti-tumor mechanisms, we hypothesized that the synergetic delivery of PTX, DSF and Cyt C could strengthen the treatment against drug-resistant tumors with high efficiency.

Cocktail therapy, also called combination chemotherapy, refers to the simultaneous integration of multiple therapeutic agents modulating the same or several anti-tumor effects, which was proposed to conquer monotherapy-induced sufficient therapeutic outcome and drug resistance[14]. With an extensive understanding of the molecular and cellular mechanisms of chemotherapeutic agents, increasing cocktail therapy candidates and strategies have been developed with enhanced therapeutic functions *via* identical or synergetic signaling pathways[15]. However, conventional cocktail therapy administrations have been evidenced with limited pharmacodynamic effects and the occurrence of MDR in clinic[16]. The modest treatment efficacy often links to the simple coadministration of multiple drugs, resulting in inconsistent pharmacokinetic behaviors[17]. The combined use of drugs cannot act synchronously on the target sites, impeding them from simultaneously exerting anti-MDR and therapeutic effects[18]. Conversely, chronic and repeated administration of defective cocktail therapies could increase side effects and exacerbate MDR status[19]. Integrating combined agents efficiently and synchronously delivering multiple drugs to target lesions is urgently needed to develop cocktail therapy for anti-MDR oncotherapy.

Nanocarriers (*e.g.*, liposomes[20], polymer micelles, albumin nanoparticles, nanoemulsions, etc.) have been widely applied to improve drug delivery and combat the MDR tumors[21-23]. However, due to their limited loading capacity, conventional nanocarriers are usually tricky to effectively co-load two or more drugs. Secondly, the limitations in adjusting the co-payload ratio on conventional nanocarriers compromise their synergistic therapeutic effect. Thirdly, due to unique characteristics of high molecular weight and readily biodegradability, biomacromolecules are hindered from being delivered to the cells. As an extensively used type of nanomedicines in clinics, pure drug nanocrystals are

carrier-free drugs with high drug-loading capability (almost up to 100%), attracting increasing attention in developing targeted drug delivery systems[24]. Based on the cocrystal strategy, nanocrystals could be designed to integrate two or more chemotherapeutic drugs with ligands by non-covalent bonds under a flexible stoichiometric ratio at the same time[25,26]. Furthermore, the nanocrystals can act like nanosized particles and effectively deliver the biomacromolecules into tumor cells[27].

Herein, a "one stone and three birds" nanococktail formulation (termed HA-HNRplex, 186 nm) was integrated by a cocrystal@protein-anchoring strategy, which PTX-DSF cocrystal-like nanorods (NRs) were anchored with the basic protein drug Cyt C, followed by hyaluronic acid (HA) modification (Fig. 1). In this study, we designed a "one stone and three birds" nanococktail formulation using cocrystal@protein-anchoring for simultaneously delivering triple drugs to combat MDR cancer. In brief, PTX/DSF cocrystals (NRs), constructed *via* anti-solvent ultrasonic precipitation method, were developed to deliver the basic protein Cyt C through electrostatic adsorption. The final nanococktail formulation of HA-HNRplex was prepared by HA coating for CD44-targeting. Among NRs, DSF can down-regulate the MDR-1 gene to reduce the expression of P-gp, thereby reducing drug efflux and improving the sensitivity of tumor cells to drugs; meanwhile, PTX is frequently used to promote tumor cell apoptosis by inhibiting microtubule depolymerization[28]. Simultaneously, Cyt C can bind with apoptotic protease activating factor-1 (Apaf-1) and caspase 9 proteins in the cytoplasm, followed by activating Pro-caspase 3 to Cleaved-caspase 3 to further promote cell apoptosis[13]. Subsequently, the anti-MDR and anti-tumor efficacy of HA-HNRplex were investigated on normal A549 and A549/Taxol drug-resistant tumor cells. Also, the *in vivo* pharmacokinetic study, biodistribution and anti-tumor efficiency of HA-HNRplex were performed on A549/Taxol drug-resistant tumor-bearing mice, respectively. Finally, collaborative mechanism was investigated by using western blotting assay and proteome analysis technique. The HA-HNRplex showed

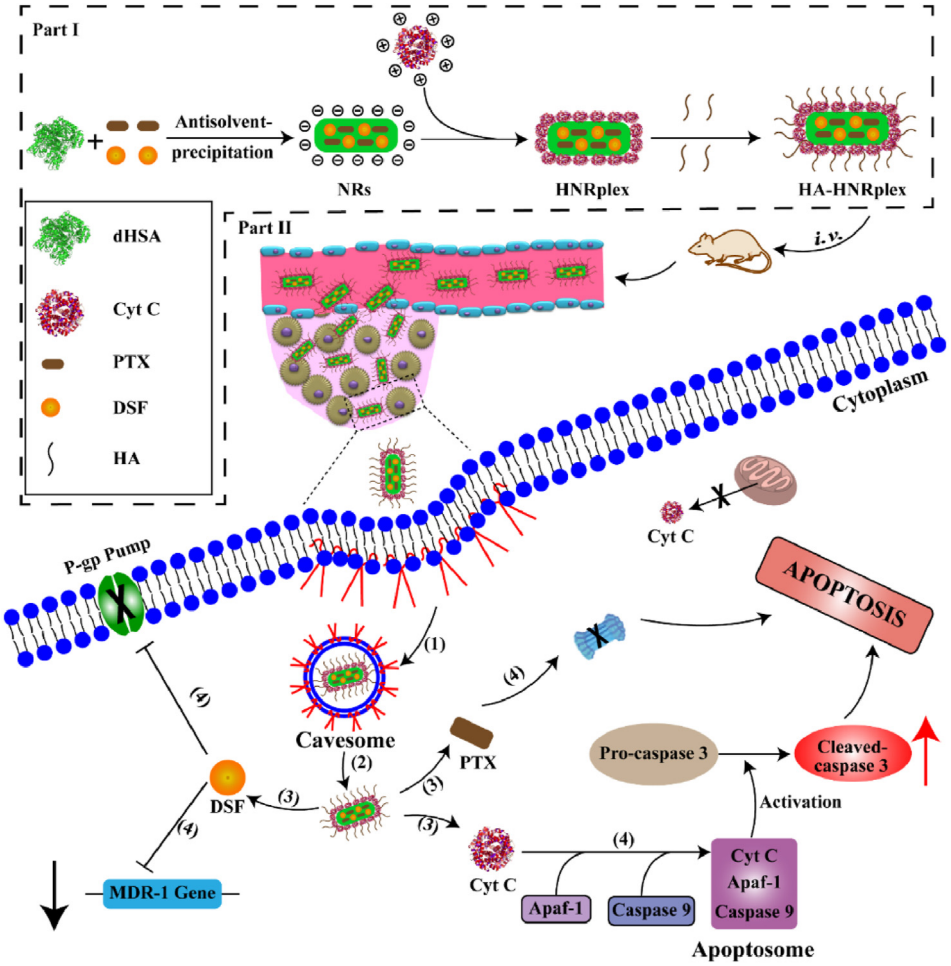

Figure 1 Schematic illustration of HA-HNRplex preparation and mechanism for "one stone and three birds" synergistic anti-tumor effects. Part I—preparation of HA-HNRplex. Part II—synergistic anti-tumor effect of HA-HNRplex *via* cascade *in vivo* fate: (1) After i.v. administration, HA-HNRplexs accumulate in tumor tissues through EPR effect, then enter tumor cells and form the cavesomes *via* the binding between HA and tumor-expressed CD44 receptors; (2) The cavesomes release HA-HNRplex into cytoplasm of tumor cells; (3) HA-HNRplex release PTX, DSF and Cyt C separately to exert synergistic anti-tumor effects; (4) The "one stone and three birds" synergistic anti-tumor effects of HA-HNRplexs are mainly attributed to three mechanisms. DSF reduces the expression of P-gp by downregulating MDR-1 gene, inhibiting drug efflux from tumor cells. PTX inhibits microtubule depolymerization to promote tumor cell apoptosis. Cyt C binds to cytoplasmic Apaf 1 and caspase 9 proteins to form apoptosome complex, activating Pro-caspase 3 to Cleaved-caspase 3 for promoting tumor cell apoptosis.

extraordinarily high encapsulation efficiency and demonstrated prolonged *in vivo* circulation and increased tumor-targeting accumulation, which could significantly reverse tumor drug resistance and improve anti-tumor efficacy. The mechanistic study demonstrated that HA-HNRplex induced the apoptosis of Taxol drug-resistant tumor cells through the signal pathway P-gp/Cyt C/caspase 3.

2. Materials and methods

2.1. Materials

PTX with more than 99% purity was purchased from Jiangsu Taxus Biotechnology Co., Ltd. (Jiangsu, China). Human serum albumin (HSA), Cyt C, DSF were purchased from Sigma−Aldrich Co., Ltd. (St. Louis, USA). Hyaluronic acid (HA) with 8000 Da and more than 98% purity was ordered from Furuida Biotechnology Co., Ltd. (Shandong, China). Chlorpromazine (CPZ) with more than 99% purity was purchased from MedChemexpress LLC (New Jersey, USA). 1-(3-Dimethylaminopropyl)-3-ethylcarbo diimide hydrochloride (EDC) was from Shanghai Aladdin Biochemical Technology Co., Ltd. (Shanghai, China). Nystatin and Methyl-β-cyclodextrin (M-CD) were purchased from Sigma−Aldrich Co., Ltd. (St. Louis, USA). 3-(4,5-Dimethylthiazol-2-yl)-2,5-diphenyltetrazolium bromide (MTT) was ordered from Jiangsu KeyGEN BioTECH Co., Ltd. (Jiangsu, China). Phosphate buffer saline (PBS), penicillin streptomycin, and trypsin were ordered from Epizyme Biomedical Technology Co., Ltd. (Shanghai, China). Fetal bovine serum (FBS) and DMEM medium were purchased from Fcmacs Biotech Co., Ltd. (Jiangsu, China). 4′,6-Diamidino-2-phenylindole (DAPI), Fluorescein isothiocyanate (FITC) and Rhodamine isothiocyanate (RITC) were purchased from Beyotime Institute of Biotechnology (Haimen, China).

The animals were purchased from Qinglong Mountain Animal Breeding Ground (Nanjing, China). All the animals were fed and cared for according to the Principles of Laboratory Animal Care and the Guide for the Care and Use of Laboratory Animals. All the related experiments were conducted under the guidelines from the Animal Ethics Committee approved protocols of China Pharmaceutical University.

2.2. Preparation and characterization of HA-HNRplex

HA-HNRplexs were constructed *via* a modified anti-solvent precipitation-ultrasonic method using denatured-HSA (dHSA) as a stabilizer[29]. In brief, 10 mg of PTX and 2 mg of DSF dissolved in 500 μL ethanol were dropwise added into 10 mL dHSA solution (1 mg/mL), following with probe ultrasonication (Scientz-IID, Ningbo Xinzhi Biotechnology Co., Ltd., Ningbo, China) at 220 W for 15 min under the ice bath. In sequence, the residual ethanol was removed from the collected suspension by spin evaporation under reduced pressure to obtain eutectic-like NRs. The obtained NRs were purified by centrifugation in ultrafiltration tube and redispersion 3 times to remove unassembled PTX, DSF and dHSA. HNRplex was prepared by dropwise adding 1 mL Cyt C (1 mg/mL) to different concentrations of NRs solution and incubated in a shaking bath for 30 min at room temperature. Finally, the HA-HNRplex was prepared by mixing HNRplex with 10 μL HA (1 mg/mL). The obtained HA-HNRplexs were purified through centrifugation and redispersion 3 times using a 3000 Da ultrafiltration tube to remove free Cyt C and HA. The dual fluorescence-labeled HA-HNRplex was fabricated *via* a similar process by replacing 1 mg of PTX with 1 mg of FITC in the system and the Cyt C with RITC-Cyt C.

The mean particle size, Zeta potential and polydispersion index (PDI) were determined by the dynamic light scattering (DLS) principle using a Malvern Zetasizer Nano-ZS90 (Size analyzer, Malvern Instruments, Malvern, UK) in triplicate at room temperature. The morphology observation of nanoparticles was performed by transmission electron microscopy (TEM, Hitachi, Ltd., Tokyo, Japan). All samples were dropped on a copper grid, followed by staining with 2% (*w*/*w*) phosphotungstic acid for 5 min. The nondenaturing gel electrophoresis was carried out to verify the loading of Cyt C and investigate the optimal d HAS/Cyt Cmass ratio *via* (Tanon EPS-300, Shangha, China) and Bio-Rad chemiluminescence imaging system (Chemidoc XRS, Bio-Rad, CA, USA). Then, Cyt C was semi-quantitated using ImageJ (National Institutes of Health, USA) software. The preparations were mixed with 10% FBS saline at 37 °C and 150 rpm to investigate storage stability.

The binding between Cyt C and NRs was investigated *via* Fluorescence Resonance Energy Transfer (FRET) assay using FITC and RITC as a fluorescent donor and an acceptor, respectively. The circular dichroism (CD) spectra analysis was recorded using a circular dichroism chromatograph (JASCO CD spectrometer, Spectrophotometer Co., Ltd., Tokyo, Japan) equipped with a temperature-controlling unit and a quartz cuvette. The measurement parameters were recorded: bandwidth, 1 nm; response, 1 s; wavelength range, 190−250 nm; scanning speed, 100 nm/min; cell length, 0.1 cm; temperature, 25 °C; protein concentration, 0.1 mg/mL.

The encapsulation efficiency and drug loading of PTX, DSF and Cyt C in HA-HNRplex were investigated by ultrafiltration-centrifugation method[30]. The free PTX, DSF and RITC-Cyt C in the HA-HNRplex were separated by centrifuging in ultrafiltration device at 3500 rpm for 30 min. The content of PTX and DSF in the supernatant collection (W_{PTX} or W_{DSF}) and the whole nanoparticles [W_{Total} (PTX or DSF)] was determined *via* high-performance liquid chromatography system (HPLC, SPD-10Avp, Shimadzu, Japan). The content of RITC-Cyt C in the supernatant collection ($W_{Cyt\ C}$) and the whole nanoparticles [W_{Total} (Cyt C)] was determined *via* RITC fluorescence. The encapsulation efficiency and drug loading were calculated with Eqs. (1) and (2) as follows:

$$\mathrm{EE}\ (\%) = \frac{W_{PTX}\ \text{or}\ W_{DSF}\ \text{or}\ W_{Cyt\ C}}{W_{Total}\ (\text{PTX or DSF or Cyt C})} \times 100 \quad (1)$$

$$\mathrm{DL}\ (\%) = \frac{W_{PTX}\ \text{or}\ W_{DSF}\ \text{or}\ W_{Cyt\ C}}{W_{Total}\ (\text{PTX} + \text{DSF} + \text{Cyt C})} \times 100 \quad (2)$$

The isolation and quantitation of PTX and DSF were conducted in a Diamonsil C18 column (4.6 mm × 250 mm, 5 mm; Dikma Technologies, Beijing, China), setting the mobile phase with the ratio of methanol/water (80:20, *v*/*v*) at 1 mL/min under different determine wavelength (PTX: 227 nm, DSF: 275 nm). RITC-labeled Cyt C was quantitated using a fluorescence spectrometer (RF-5000, Shimadzu, Kyoto, Japan) to test the RITC intensity.

2.3. In vitro drug release

The release behavior of PTX, DSF and Cyt C was assessed by a dialysis method at different mediums (pH 7.4, 6.8 and 5.5). In brief, 2 mL HA-HNRplex was transferred into a dialysis bag (MWCO 3500 Da), incubated in PBS release media with 0.5% tween and placed in a water bath shaker (SHA-C, Jintan, China) under 100 rpm, 37 °C. At specific time intervals, 300 μL release medium of different samples was sampled, followed by replenishing an equal volume of fresh medium, respectively. After filtration through 0.45 μm microporous membranes, the concentration of PTX and DSF in filtrates was determined by the HPLC system (SPD-10Avp, Shimadzu, Kyoto, Japan). For investigation of Cyt C release, 2 mL RITC-labeled HA-HNRplex was transferred into a dialysis bag (MWCO 300 kDa), immersed in the same PBS medium (pH 7.4, pH 6.8 and pH 5.5) and incubated under the same condition as above. At specific time points, 500 μL release medium and an equal volume of fresh medium were sampled. The RITC-Cyt C was quantified by measuring the RITC intensity *via* a fluorescence spectrometer (RF-5000, Shimadzu, Kyoto, Japan). The cumulative release percentage of different drugs was calculated with Eq. (3) as follows:

$$\text{Cumulative release}\ (\%) = \frac{C_r}{C_t} \times 100 \tag{3}$$

C_r was the concentration of drugs in the sampled release medium and C_t represented the total concentration of drugs in preparation.

2.4. Cell culture

The A549 cells and A549/Taxol cells (Taxol-resistant cell line) were cultured in DMEM medium with 10% FBS and 1% penicillin−streptomycin in the incubator at 37 °C, 5% CO_2. The cells were harvested with 0.25% trypsin and seeded in a cell culture plate with an appropriate density of the cell suspension for further investigations. The Taxol-resistance of A549/Taxol cells compared to normal A549 was evaluated by treating with a series of Taxol concentrations.

2.5. Cellular uptake

The cellular uptake study was comprehensively investigated by confocal laser scanning microscope (CLSM, LSM800, Zeiss, Oberkochen, Germany). In brief, A549 cells and A549/Taxol cells were seeded and cultured in 12-well plates at 2×10^5 cells/well density and cultured for another 24 h. Then, the previous cell culture medium was discarded and added to a fresh culture medium containing RITC-labeled preparations (10 μg/mL) at 37 °C for 0.5, 1, 2, 4, and 6 h, respectively. After incubation, the cells were washed with cold PBS 3 times and digested with 0.25% trypsin. The A549 and A549/Taxol cells were resuspended in PBS for flow cytometry analysis using FACSCalibur (BD, Franklin Lake, USA) to measure the fluorescence intensity. CLSM was performed to observe further the cellular uptake behavior of A549 and A549/Taxol cells. In brief, cells were seeded at a density of 2×10^5 cells in specific dishes (ThermoFisher Scientific, USA) for 24 h, incubated with 200 μL RITC-FITC dual-labelled preparations (10 μg/mL), fixed with methanol for 10 min, stained with DAPI for 15 min, and observed under CLSM (LSM800, Zeiss, Oberkochen, Germany).

For the mechanism study of the internalization pathway, A549 and A549/Taxol cells were pre-incubated with different uptake inhibitors for 0.5 h, including chlorpromazine (CPZ, 10 mg/mL), nystatin (10 μmol/L) and methyl-β-cyclodextrin (M-β-CD, 2.5 mmol/L). Then, the endocytosis mechanism was investigated *via* flow cytometry analysis and CLSM observation according to the above experimental process.

2.6. In vitro cytotoxicity and apoptosis

The cytotoxicity and cell viability were evaluated by the MTT assay. In brief, A549 and A549/Taxol cells were seeded and cultured at a density of 2×10^5 cells/mL in a 96-well plate for 24 h, incubated with different preparations at various drug concentrations for another 24 h at 37 °C. Subsequently, treated cells were cultured with 20 μL of MTT (5 mg/mL) for 4 h and added with 200 μL DMSO. The cell viability was determined by a microplate reader (ThermoFisher Scientific, Waltham, USA) at the absorbance of 570 nm.

Cell apoptosis study was investigated using Annexin V-FITC/PI apoptosis kit measured *via* flow cytometry. In brief, A549 and A549/Taxol cells were seeded at a density of 1×10^5 cells/mL in a 12-well plate and cultured for 48 h. Then, cells were incubated with different preparations for 24 h and washed with cold PBS for 3 times. After that, the treated cells were collected after digestion and marked with Annexin V-FITC/PI apoptosis kit according to the protocol, quantified by flow cytometry (FACSCalibur, BD, Franklin Lake, USA).

2.7. Western blotting assay (WB)

The WB assay was conducted to evaluate the expression of Cyt C and Cleaved-caspase 3. In detail, cells or tissues were precipitated by centrifugation (12,000×g, 20 min) and incubated in cold RIPA lysis buffer (50 μL) with protease inhibitor in an ice-water bath for 30 min, following centrifugation again to collect the supernatant. The protein of samples was quantified by a BCA protein assay kit and separated by SDS-PAGE, then transferred to a polyvinylidene difluoride (PVDF) membrane and incubated with a blocking solution. Then, PVDF membranes were incubated with primary monoclonal antibodies, including Cyt C (1:2000, CST), cleaved-caspase 3 (1:3000, Abcam) and β-actin (1:3000, Abcam) overnight at 4 °C and horseradish peroxidase (HRP) secondary antibody for 1 h. Finally, the collected bands were stained with an ECL chemiluminescence kit (Tanon, Shanghai, China) and exposed to an automatic chemiluminescence imaging detection system (Tanon, Shanghai, China). The band images were quantified *via* ImageJ (NIH, Bethesda, MD, USA) to evaluate the expression of proteins.

2.8. Pharmacokinetic study

For *in vivo* pharmacokinetic investigation, DiR-labeled preparations (1.5 mg/kg), free DiR, DiR-HNRplex and DiR-HA-HNRplex were administrated to SD rats (180−250 g) according to body weight *via* tail veins. 0.5 mL blood was collected from orbit at 15 min, 30 min, 1, 2, 4, 6, 8, 10 and 24 h respectively, and centrifugated at 3000 rpm (TDZ5-WS, Xiangyi, Hunan, China) for 10 min to obtain serum. The concentration of DiR (DiR-labeled preparations) was quantified by measuring fluorescence intensity *via* a multifunctional microplate reader (ThermoFisher Scientific,

USA). The pharmacokinetic parameters of different groups were calculated by Winnonlin 7.0 software (Pharsight, CA, USA) under noncompartmental analyses.

2.9. A549/Taxol tumor-bearing models

A549/Taxol tumor-bearing mice were established by subcutaneous injection of A549/Taxol cells (in logarithmic growth phase) at a density of 1×10^6 per mouse (0.2 mL) at the left armpit. The blank control group is the normal mice without injection of A549/Taxol cells. In our study, nude mice were used for better observation of tumor growth and biodistribution of preparations, while BALB/c mice were used for pharmacodynamic investigation. Preparations or vehicles were administrated to A549/Taxol tumor-bearing mice when the tumor volume reached 500 mm^3.

2.10. In vivo living image and biodistribution

The A549/Taxol tumor-bearing mice with 300−500 mm^3 tumor volume were administered with free DiR, DiR-HNRplex, and DiR-HA-HNRplex *via* tail veins (DiR dose of 1 mg/kg), respectively. The treated mice were anesthetized and imaged at 2, 4, 8, 12 and 24 h by IVIS Spectrum imaging system (PerkinElmer, MA, USA). The Ex and Em wavelengths of DiR channels were set as 730 and 790 nm. At the end of the last time point, the mice were sacrificed and the major tissues, including tumor, liver, heart, lung, spleen and kidney, were collected for *ex vivo* imaging under the same method.

2.11. In vivo anti-tumor study

After the mean tumor volume of A549/Taxol tumor-bearing mice reached 150 mm^3, the animals were randomly divided into 5 groups ($n = 6$), including saline group, PTX-DSF PM group, NRs group, HNRplex group and HA-HNRplex group. The mice were administrated with diverse preparations (0.2 mL) i.v. at a dosage of 10 mg/kg PTX, 2 mg/kg DSF and 1 mg/kg Cyt C every two days 5 times (Days 0, 2, 4, 6, 8, and 10). The tumor sizes were measured and recorded before each administration. All mice were sacrificed on Day 11 to collect tumors and other major tissues for further investigations.

2.12. Determination of Cyt C and Cleave-caspase 3 in tumor tissues

The expression of Cyt C in tumor tissues was evaluated using WB assay. In detail, 15 mg tumor tissues of different groups (Saline group, PTX-DSF PM group, NRs group, HNRplex group and HA-HNRplex group) were mixed with 300 μL of RIPA lysis solution in a tissue grinder with lysis on ice for 15−30 min. The total protein was extracted after centrifugation and quantified by BCA protein assay kit. Then, the proteins were separated by SDS-PAGE, transferred to a polyvinylidene difluoride (PVDF) membrane, and incubated with a blocking solution. After incubating with primary monoclonal antibodies including Cyt C (1:2000, CST), cleaved-caspase 3 (1:3000, Abcam) and β-actin (1:3000, Abcam) overnight at 4 °C and horseradish peroxidase (HRP) secondary antibody for 1 h, the samples were stained with ECL chemiluminescence kit and exposed to automatic chemiluminescence imaging detection system. The β-actin was used as a standardized internal reference and the images were quantified *via* ImageJ software to evaluate the expression of Cyt C and Cleave-caspase 3.

2.13. Histological analysis

Histological analysis of the tumor tissues was conducted by hematoxylin-eosin (H&E) staining, Ki67, and TUNEL staining to evaluate the pathomorphological changes and cell apoptosis after treatment, respectively. In short, after being fixed in 4% paraformaldehyde for 24 h, the tumor tissues of diverse groups (Saline, PTX-DSF PM, NRs, HNRplex and HA-HNRplex group) were embedded in paraffin and cut into 1.5 cm × 1.5 cm sections for H&E staining. The sections were carried out according to the standard instructions for immunohistochemistry studies, followed by incubation with anti-Ki67 (1:450, Abcam, Cambridge, England) primary antibody at 4 °C overnight. The sample slides were washed and incubated with the specific secondary antibodies at 37 °C for 30 min and calculated *via* Image-Pro Plus 6.0 software. The TUNEL assay was conducted to evaluate the apoptosis of tumor cells. Briefly, the TUNEL staining cell apoptosis detection kit (KeyGEN, Nanjing, China) was used to distinguish apoptotic cells labeled with red fluorescence. The apoptosis rate was calculated by determining the number of TUNEL-positive cells under a microscope within 6 random fields on total cells.

2.14. Statistical analysis

All data were presented as the means ± standard deviation (SD) and the statistical analysis were assessed using GraphPad Prism 9.0 to calculate significant difference between different groups. The Student's *t*-test was utilized to compare the means of two groups, whereas the one-way ANOVA was assessed in comparing more than two groups. $P < 0.05$ was considered a significant difference.

3. Results

3.1. Preparation and characterization of HA-HNRplex

Three steps were involved in preparing HA-HNRplex (Fig. 2A). First, the cocrystal NRs of PTX and DSF were fabricated by a modified anti-solvent precipitation-ultrasonic method[31]. Thermally dHSA was used as a stabilizer after a 90°C-heating in a water bath for 2 h. Different types of organic solvents have the potential to affect the self-assembly of PTX, DSF and dHSA. Ethanol, acetone and DMSO were investigated for the NR preparation. The formulation prepared by ethanol was selected for further study because the constructed NRs showed the smallest particle size and greater than 20 mV absolute potential value (Supporting Information Table S1). Changing the mass ratio of PTX:DSF and the drug loading of PTX could also influence the properties of obtained NRs. As shown in Fig. 2B and C, and Supporting Information Fig. S1, when the mass ratio of PTX:DSF was 5:1, while the PTX loading at 10 mg, the prepared NRs demonstrated optimal characteristics with the smallest particle size of 148 ± 2.45 nm and the most considerable absolute potential value of −23 ± 1.75 mV. TEM observation illustrated that the PTX-DSF NRs exhibited a rod-like crystal structure shape with a 100−180 nm particle length, consistent with the DLS results (Fig. 2D). The circular dichroism spectrum results revealed the alteration in the secondary structure of the dHSA protein in NRs, indicating the interactions between drug molecules (PTX and DSF) and dHSA with concentration-dependent phenomenon (Fig. 2E). Meanwhile, the fluorescence spectroscopy was used to

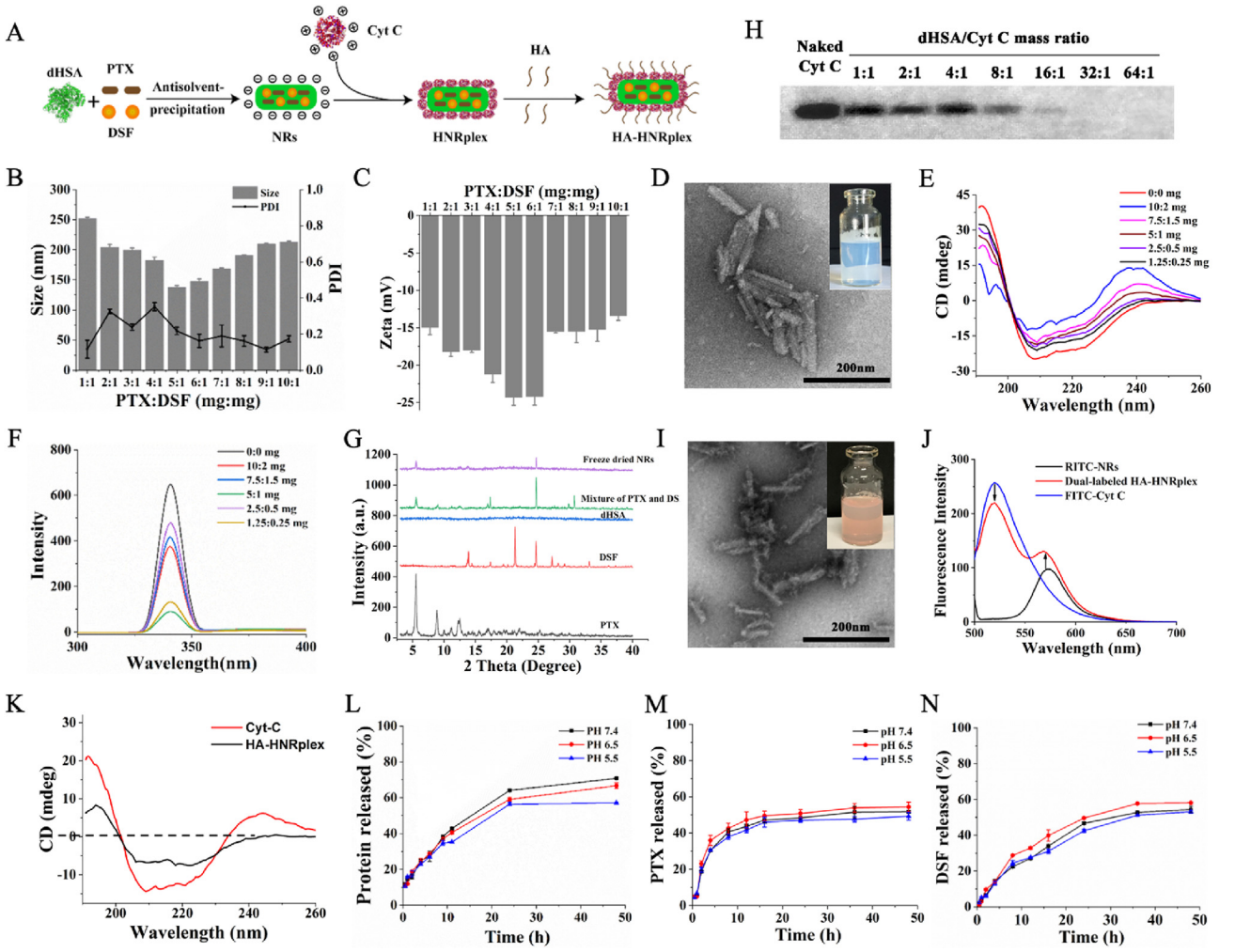

Figure 2 Preparation and characterization of HA-HNRplex. (A) Schematic illustration for the preparation of HA-HNRplex. (B) Particle size and PDI of PTX/DSF NRs in different PTX/DSF ratio under the measurement of DLS. (C) Zeta potential of PTX/DSF NRs in different PTX/DSF ratio. (D) TEM image of PTX/DSF NRs and digital picture of the nanoparticle dispersion. (E) CD and (F) fluorescence spectra of dHSA under different drug loading of PTX and DSF (PTX:DSF = 5:1,*w*/*w*). (G) PXRD pattern of PTX, DSF, dHSA, physical mixture and freeze-dried NRs. (H) Native PAGE study of Cyt C loaded onto HA-HNRplex under different dHSA/Cyt C mass ratio. (I) TEM image of HA-HNRplex and digital picture of the nanoparticle dispersion. (J) FRET between RITC-NRs and FITC-dHSA in HA-HNRplex. (K) CD spectra of Cyt C in preparations. *In vitro* release profile of (L) Cyt C, (M) PTX and (N) DSF from HA-HNRplex under different pH conditions at 37 °C for 48 h. Data are presented as mean ± SD (n = 3).

verify the interactions between dHSA and PTX/DSF in NRs. As shown in Fig. 2F, the fluorescence intensity of dHSA (Ex = 295 nm, Em = 340 nm) changed with the increasing amount of PTX/DSF in formulation, mainly owing to that the interactions between dHSA and hydrophobic PTX/DSF impacted the conformation of tryptophan residues in dHSA. Furthermore, PXRD examination demonstrated that dHSA contributed to the construction of PTX/DSF NRs formulation with a crystalline structure and strong stability (Fig. 2G). Additionally, the diameter of NRs was minimally altered in 10% serum after 12-h incubation, further suggesting that NRs possessed good stability for afterward study (Supporting Information Fig. S2). Finally, the driving force for the construction of nanococrystals was evaluated *via* molecular docking study and binding disruption evaluation. As shown in results of molecular docking (Supporting Information Fig. S3), strong hydrogen bonding interactions existed between PTX (red) and HSA (white). DSF (blue) demonstrated no hydrogen bonding interactions with HSA, but existed strong hydrogen bonding interaction with PTX. The evaluation of the binding disruption further confirmed that the hydrogen bonding interaction is the main molecular interaction forces between PTX, DSF and HAS (Supporting Information Fig. S4).

Next, NRs were used as "carriers" to load the basic protein Cyt C, developing NRs/Cyt C complex (HNRplex) by electrostatic interaction between NRs (negative charge) and Cyt C (positive charge under physiological conditions). The native-PAGE results indicated that the PAGE bands of Cyt C were not determined upon the mass ratio of dHSA/Cyt C ≥ 16, indicating that Cyt C was loaded onto NRs (Fig. 2H). Therefore, the 16:1 was selected as the optimal dHSA/Cyt C mass ratio to prepare HNRplex.

Finally, HNRplex was modified with HA for CD44-targeting[32]. As shown in Supporting Information Table S2, the particle size of HA-HNRplex expanded gradually with the increase of HA content. Among the formulations, the HA-HNRplex at 16:1:0.5 mass

ratio of dHSA/Cyt C/HA, with a particle size of 186.12 ± 1.04 nm and a potential of −10 ± 0.68 mV (Table S2), was chosen as the optimal preparation for further study owing to its suitable particle size (<200 nm) and high HA loading. The loading and encapsulation efficiency of drugs in HA-HNRplex were determined by the ultrafiltration method. From Supporting Information Table S3, HA-HNRplex demonstrated high total drug loading of up to 54.5% (*w*/*w*), and high EE/DL of 98.01 ± 0.29%/43.22 ± 0.38% for PTX, 96.71 ± 0.11%/8.53 ± 0.23% for DSF, ≈100 %/2.75 ± 0.13% for Cyt C, respectively. The TEM observation revealed that the morphology of HA-HNRplex was similar to that of NRs with a rod-like structure and 150−200 nm in length (Fig. 2I). Especially, the surface of HA-HNRplex showed a granular phenomenon due to the adsorption of the basic protein and targeting modifications. The conjugation of NRs and Cyt C was confirmed by the FRET (fluorescence resonance energy transfer), as the donor fluorescence molecules in the excited state can transfer energy to the receptor fluorescence molecules, resulting in a decrease in the fluorescence intensity of the donor and an increase in the fluorescence intensity of the receptor. As shown in Fig. 2J, the fluorescence intensity of dual-fluorescent-labeled HA-HNRplex decreased at the FITC Em wavelength of 520 nm than FITC-Cyt C with the same concentration, at the same time, the fluorescence intensity of HA-HNRplex increased at the RITC Em wavelength of 590 nm compared to the same concentration of RITC-NRs alone, proving the existence of FRET effect and the conjugation of NRs and Cyt C. Also, the alteration in the secondary structure of the Cyt C protein in HA-HNRplex measured *via* CD spectrum indicated the conjugation of NRs and Cyt C, corresponding to the FRET study (Fig. 2K). The particle size of HA-HNRplex was not significantly changed after 12-h incubation in 10% FBS, indicating the potential solid stability of the nanoparticles (Supporting Information Fig. S5).

The *in vitro* release study showed that HA-HNRplex continuously released Cyt C in a 48-h duration. Meanwhile, the protein release at pH 7.4 was faster than at pH 5.5 because the higher pH value medium could reduce the net positive charge of the basic protein and compromise the electrostatic interaction between Cyt C and NR[33] (Fig. 2L and Fig. S5). The release of two small molecule drugs was not affected by pH conditions and was less than 60% within 48 h. The slow release of the three payloads from the nanoparticles indicated the potential prolonged treatment efficacy and stable structure.

3.2. Targeted cellular uptake of HA-HNRplex to A549 and A549/Taxol cells

The nanoparticles often should transport into the tumor cells to exhibit anti-tumor function; thus, we first-in-all evaluated the targeted cellular uptake of HA-HNRplex by human lung adenocarcinoma cells-A549 and the corresponding Taxol-resistant cell line A549/Taxol *via* CLSM and flow cytometry. HA-HNRplex was dual-labeled by RITC (red) and FITC (green) to investigate cellular co-localization after internalization. For both A549 and A549/Taxol cell lines, the CLSM results showed that the intracellular fluorescence intensity of HA-HNRplex intensified with increasing incubation time in a 6-h period (Fig. 3A and F). In addition, the quantitative analysis measured by flow cytometry displayed that intracellular fluorescence increased with extended incubation time (Fig. 3B, C, G and H) and drug concentrations (Fig. 3D, E, I and J). These results suggested that the uptake of HA-HNRplex was time- and -concentration-dependent. Also, both two types of cells were confirmed with the over-expressed CD44 receptors (Supporting Information Fig. S6). Thus, among them, the significantly enhanced uptake of HA-HNRplex by cells than RITC-Cyt C was probably attributed to the targeted bind of HA-CD44 and the superiority of the NRs as "nanocarriers", effectively improving the intercellular delivery.

Of note, compared to the normal A549 cells, A549/Taxol drug-resistant tumor cells possessed the drug efflux ability to reduce the cellular uptake capacity of drugs[34]. However, our data demonstrated similar uptake levels of preparations by A549 cells and A549/Taxol cells. The results demonstrated that the HA-HNRplex could effectively inhibit the drug efflux by drug-resistant tumor cells and improve targeted delivery efficiency.

3.3. Endocytosis mechanisms of HA-HNRplex

A549 and A549/Taxol cells were pre-incubated with uptake pathway inhibitors, including CPZ (clathrin-mediated pathway inhibitor), nystatin and M-β-CD (caveolin/lipid-raft uptake inhibitor)[35], to investigate the endocytosis mechanism of HA-HNRplex. CLSM examination showed little nanoparticle uptake reduction in CPZ-pretreated A549 and A549/Taxol cells (Fig. 4A and C). In contrast, the nanoparticle uptake significantly declined in groups pretreated by nystatin or M-β-CD. Quantitative analysis confirmed that the uptake of CPZ, Nystatin, and M-β-CD treated A549 cells (Fig. 4B) were reduced by 90%, 45% ($P < 0.001$), and 36% ($P < 0.001$) than the control, while the uptake of A549/Taxol cells (Fig. 4D) were reduced by 96%, 40% ($P < 0.001$), and 58% ($P < 0.001$), respectively. These results suggested that HA-HNRplex uptake by A549 and A549/Taxol cells mainly dependent on the caveolin/lipid-raft pathway. Previous studies proved that caveolin/lipid-raft-mediated internalization allowed the nanoparticles to avoid endo-lysosome detainment[31,36]. Examination of lysosomal-colocalization demonstrated that the nanoparticles showed almost non-colocalization with LysoTracker-labeled lysosome at 1, 4 and 6 h (Supporting Information Fig. S7). This non-endo-lysosomal endocytosis of HA-HNRplex based on caveolin/lipid-raft was promising to improve the intracellular delivery of protein drugs.

3.4. In vitro cytotoxicity and improved apoptosis effect

Firstly, we examined the drug resistance of A549 cells and A549/Taxol. As illustrated in Fig. 5A, after being administered with a gradience concentration of Taxol for 24 h, the cell viability of A549/Taxol cells was significantly higher than that of normal A549 cells. Also, the IC_{50} value of A549/Taxol was nearly three times higher than that of A549 cells (Fig. 5B). The data suggested that A549/Taxol cells were resistant to Taxol.

Next, the cytotoxicity was investigated using an MTT assay. As shown in Fig. 5C and D, the NRs, HNRplex and HA-HNRplex demonstrated concentration-dependent cytotoxicity against A549 cells when the concentrations of PTX and Cyt C ranged in 0.3125−30 μg/mL and 0.0625−6 μg/mL, respectively. Little cytotoxicity was observed in the free Cyt C-treated group, mainly attributed to the poor membrane penetration of the protein and instability in endo-lysosomes[37]. Cyt C-loaded HNRplex and HA-HNRplex demonstrated significantly higher cytotoxicity than free Cyt C and NRs, proving the improved intracellular Cyt C delivery and the enhanced anti-tumor effect by the combination of PTX, DSF and Cyt C. Also, the cytotoxicity of HA-HNRplex was significantly more potent than HNRplex due to

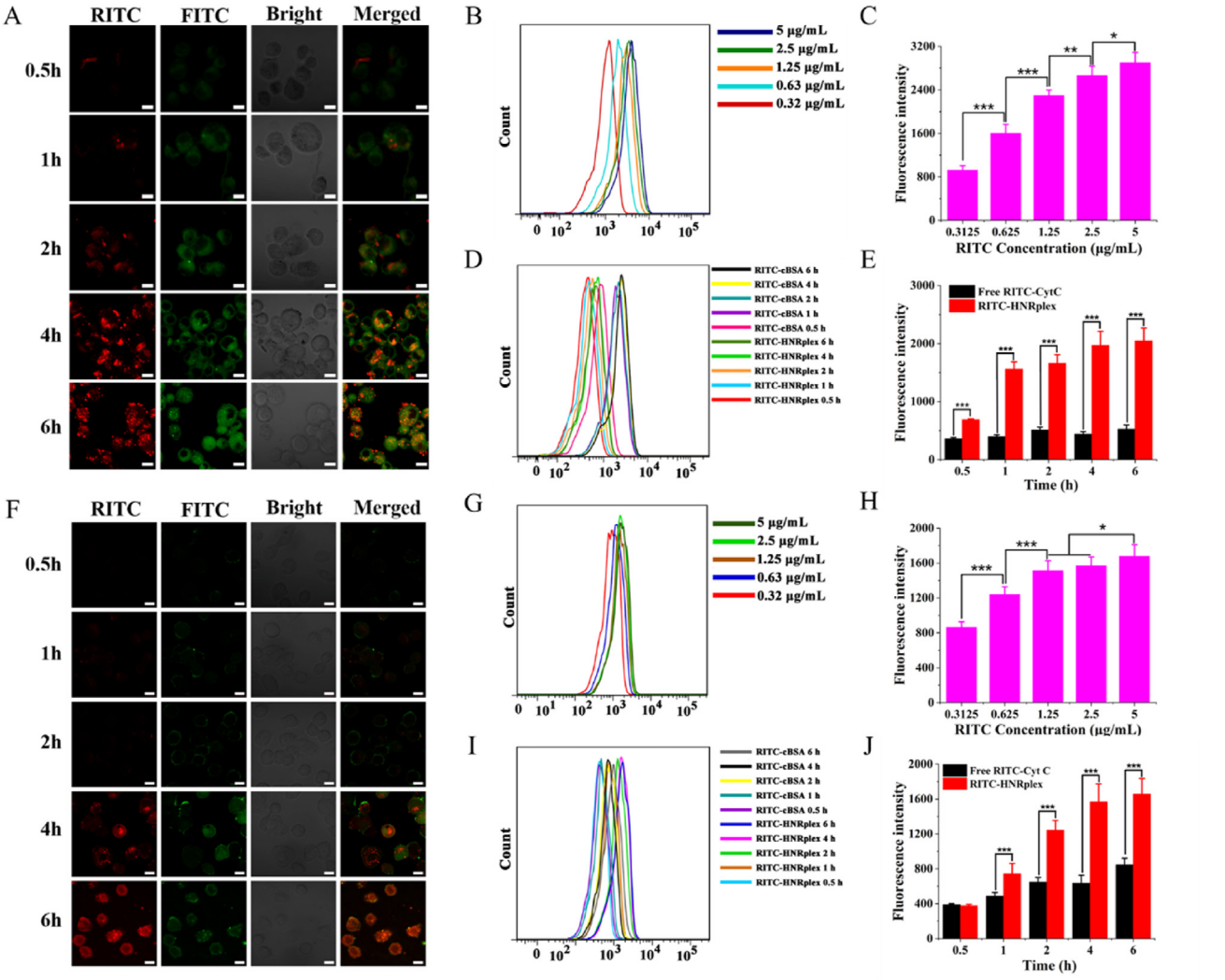

Figure 3 Cellular uptake of HA-HNRplex on A549 and A549/Taxol tumor cells. (A) CLSM images of A549 cells incubated with RITC and FITC dual-labeled HA-HNRplex at 37 °C for various durations (RITC: red, FITC: green). The scale bar is 20 μm. (B, C) Quantitative analysis of A549 cellular uptake measured by flow cytometry after HA-HNRplex treatment with different concentrations. (D, E) Quantitative analysis of A549 cellular uptake measured by flow cytometry after HA-HNRplex treatment for various durations. (F) CLSM images of A549/Taxol cells incubated with RITC and FITC dual-labeled HA-HNRplex at 37 °C for various durations (RITC, red; FITC, green). (G, H) Quantitative analysis of A549/Taxol cellular uptake measured by flow cytometry after HA-HNRplex treatment with different concentrations. (I, J) Quantitative analysis of A549/Taxol cellular uptake measured by flow cytometry after HA-HNRplex treatment for various durations. Data are presented as mean ± SD ($n = 5$). *$P < 0.05$, **$P < 0.01$, ***$P < 0.001$.

the enhanced drug delivery resulting from the ligand-receptor affinity of HA-CD44[38]. Of note, A549/Taxol cells were drug-resistant; however, the three nanoparticles demonstrated similar cytotoxicity with normal A549 cells. The results could be explained by the fact that the encapsulated DSF alleviated the drug resistance by reducing the drug efflux activity and improving the sensitivity of cells to PTX and Cyt C. These results indicated that the targeted nanococktail could effectively kill drug-resistant cancer cells.

Then, the apoptosis of tumor cells induced by various formulations was evaluated *via* Annexin V-FITC/PI assay on A549 and A549/Taxol cell lines, respectively. The apoptosis rates of A549 cells treated by Cyt C, PTX, DSF, PTX-DSF, NRs, HNRplex, and HA-HNRplex were about 0.8, 4, 4.2, 5, 5.5, 6.2, and 7 times higher than control group, respectively (Fig. 6A and B). Notably, the administration of NRs, HNRplex, and HA-HNRplex induced similar apoptosis rates on A549/Taxol drug-resistant cells, for 58%, 62% and 64%, respectively (Fig. 6C and D). Among them, compared with the free-drug groups and two-drug-treated groups (PTX-DSF physical mixture and NRs), the triple-payload nanoparticles, HA-HNRplex and HNRplex, revealed significant apoptosis-inducing ability on A549/Taxol drug-resistant cells. Again, the data indicated that the targeted nanococktail could promote the apoptosis of Taxol-resistant cancer cells.

3.5. *Intracellular Cyt C and cleaved-caspase 3 assay*

Increasing evidence has verified that Cyt C can bind with cytoplasmic Apaf 1 and caspase 9 to form Cyt C-Apaf 1-caspase 9

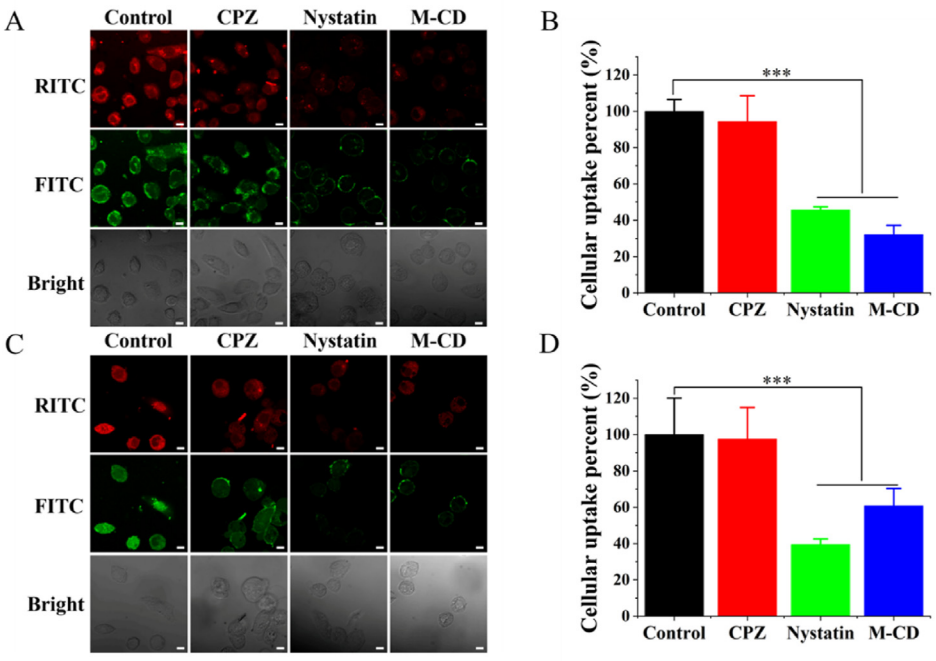

Figure 4 Endocytosis mechanism of HA-HNRplex. (A) Qualitative and (B) quantitative analysis of endocytosis mechanism of HA-HNRplex on A549 cells. A549 cells were pre-incubated with chlorpromazine (CPZ, 10 mg/mL), nystatin (10 μmol/L) and methyl-β-cyclodextrin (M-β-CD, 2.5 CF) uptake inhibitors for 0.5 h. Then the endocytosis was investigated *via* CLSM observation and flow cytometry. (C) Qualitative and (D) quantitative analysis of HA-HNRplex endocytosis on A549/Taxol cells. The experimental process on A549/Taxol cells was the same as on A549 cells. The scale bar is 20 μm. RITC: red, FITC: green. Data are presented as mean ± SD ($n = 5$). $^{*}P < 0.05$, $^{**}P < 0.01$, $^{***}P < 0.001$.

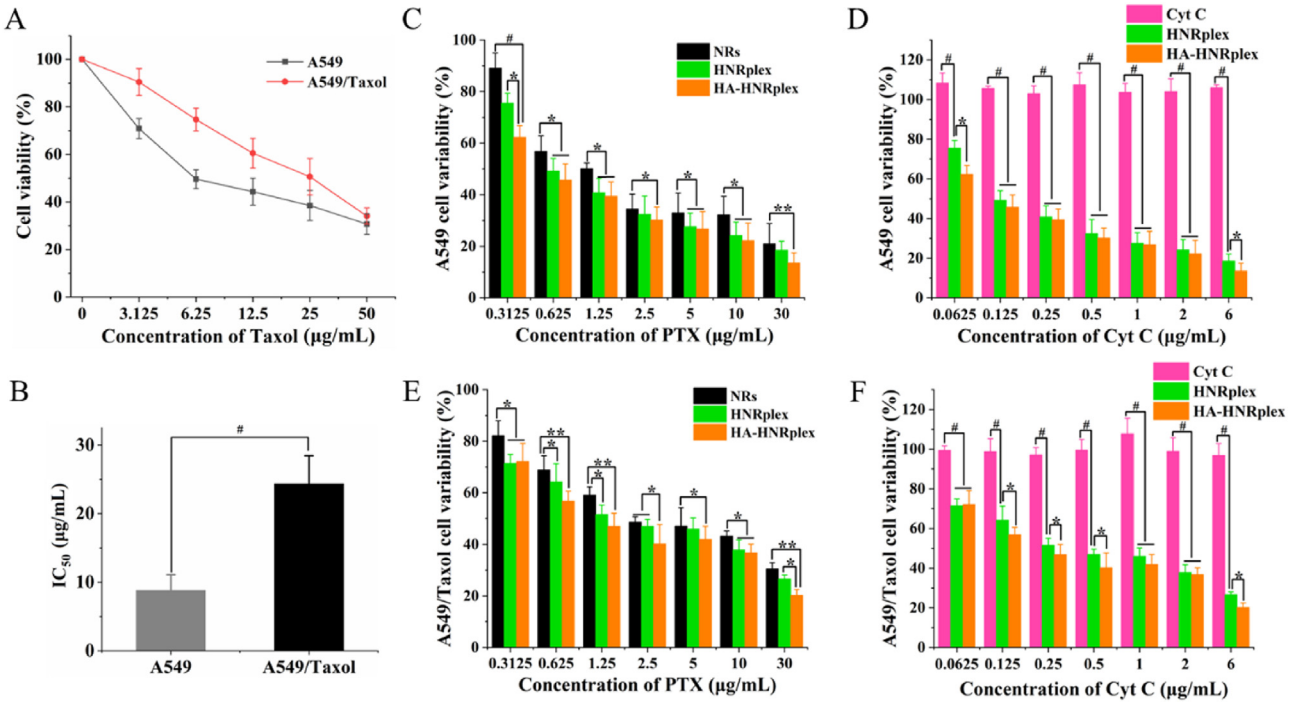

Figure 5 *In vitro* anti-tumor study. (A) Cell viability and (B) IC_{50} of A549 and A549/Taxol cells after treatment with different concentrations of Taxol. (C) Cytotoxicity of preparations to A549 under different concentrations of PTX. (D) Cytotoxicity of preparations to A549 under different concentrations of Cyt C. (E) Cell viability of A549/Taxol after treatment with preparations under PTX different concentrations. (F) Cell viability of A549/Taxol after treatment with preparations with different concentrations of Cyt C. The mass ratio of PTX:DSF in all preparations is 5:1. Data are presented as mean ± SD ($n = 5$). $^{*}P < 0.05$, $^{**}P < 0.01$, $^{\#}P < 0.001$.

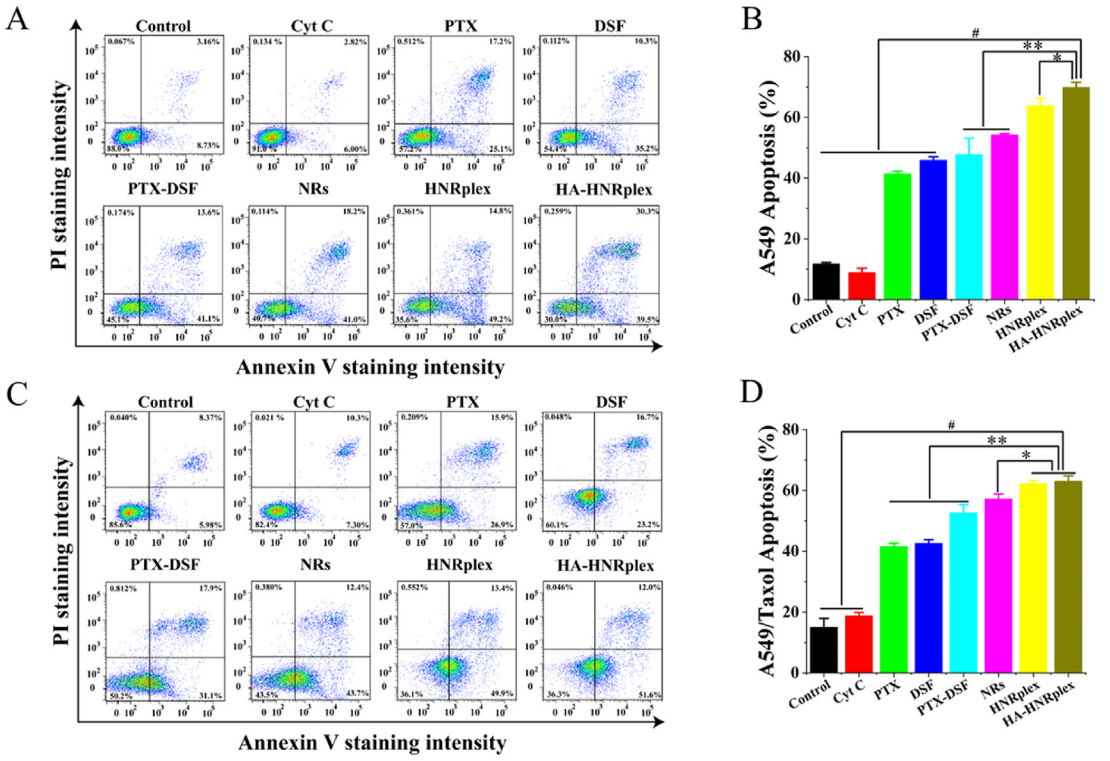

Figure 6 Improved apoptosis effect on A549 and A549/Taxol cells. (A) Qualitative and (B) quantitative analysis of A549 apoptosis measured by flow cytometry after 24-h treatment with preparations. (C) Qualitative and (D) quantitative analysis of A549/Taxol apoptosis measured by flow cytometry after 24 h-incubation with preparations. The mass ratio of PTX:DSF in all preparations is 5:1. The concentration of PTX, DSF and Cyt C was 5, 1 and 0.31 μg/mL, respectively. Data are presented as mean ± SD ($n = 5$). *$P < 0.05$, **$P < 0.01$, #$P < 0.001$, compared to HA-HNRplex group.

apoptosome, activating Pro-caspase 3 to Cleaved-caspase 3 *via* ATP and dATP, thereby promoting cell apoptosis[39] (Fig. 7A). Herein, the expression of intercellular Cyt C and Cleaved-caspase 3 after treated with different preparations was determined by WB assay. As illustrated in Fig. 7B and C, the quantification data showed that the expression of Cyt C in A549 cells was 1.2, 1.35, 1.4, 1.7, and 1.9-fold higher than the control group after incubation with PTX, DSF, PTX-DSF, NRs, HNRplex, and HA-HNRplex. Consistently, in the resistant cells (Fig. 7E and F), the expression of Cyt C was measured to 1.26, 1.35, 1.4, 1.75, and 1.96-fold greater than the control after the same treatment. Among all the groups, the HA-HNRplex group exhibited the highest expression of Cyt C. The results indicated that HA-HNRplex promoted the intracellular delivery of Cyt C in A549 cells and A549/Taxol drug-resistant cells.

The intracellular Cyt C enables the activation of caspase 3 proenzyme and upregulation of Cleaved-caspase 3, promoting apoptosis of tumor cell (Fig. 7A). Quantification analysis of WB revealed that the expression of Cleaved-caspase 3 in A549 cells was 1.2, 1.35, 1.4, 1.7, 1.75, and 1.98-fold higher than control after the treatment of PTX, DSF, PTX-DSF, NRs, HNRplex, and HA-HNRplex, respectively (Fig. 7B and D). Similarly, A549/Taxol cells expressing Cleaved-caspase 3 were 1.15, 1.2, 1.4, 1.35, 1.5, and 1.7-fold higher than the control after treatment (Fig. 7E and G). Among them, the highest expression of Cleaved-caspase 3 was found in the HA-HNRplex group. As a result, our data on the molecular study indicated that the HA-HNRplex strengthened the activation of the caspase 3 proenzyme and then upregulated Cleaved-caspase 3.

3.6. Pharmacokinetics and tumor-targeted distribution of HA-HNRplex system

The sufficient circulation time of a delivery system is a prerequisite, allowing them to accumulate in the targeted tumor tissues[40]. First, the pharmacokinetics of DiR-labeled formulations were investigated in rats after tail vein intravenous administration. As illustrated in Supporting Information Fig. S8, the HA-HNRplex and HNRplex demonstrated similar circulation behavior observed on the plasma concentration−time curves. In contrast, compared to free DiR, HA-HNRplex and HNRplex exhibited a higher DiR-plasma concentration measured within a 24-h period. The pharmacokinetic parameters verified that the two nanoparticles had improved *in vivo* behavior, as shown by prolonged half-lives and increased bioavailability (Supporting Information Table S4).

Then, the tumor-targeted distribution of preparations was evaluated *via in vivo* fluorescence imaging on A549/Taxol tumor-bearing nude mice after intravenous injection of free DiR, DiR-HNRplex and DiR-HA-HNRplex. As shown in Fig. 8A, the fluorescence intensity of DiR-HA-HNRplex and DiR-HNRplex accumulated at the tumor site increased within 24 h, while free DiR demonstrated almost non-fluorescence in the tumor and mainly distributed in the liver, kidney, and lung. Quantitative analysis data of fluorescence image indicated that the accumulation of HA-HNRplex in tumor tissues was significantly higher than DiR-HNRplex and free DiR (Fig. 8B). The enhanced tumor distribution of HA-HNRplex was mainly attributed to prolonged *in vivo* circulation and efficient tumor-targeted delivery mediated

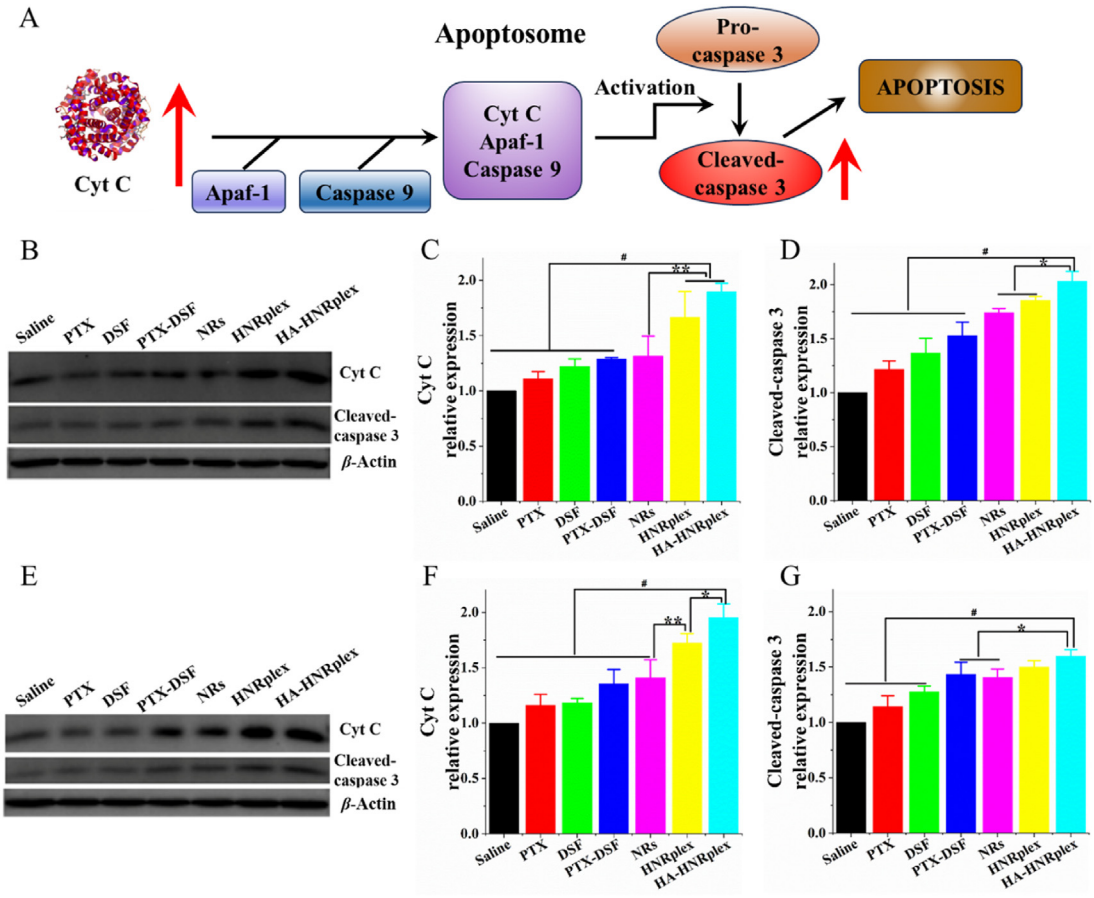

Figure 7 The levels of Cleaved-caspase 3 and Cyt C in preparation-treated A549 and A549/Taxol cells. (A) Schematic illustration of Cyt C-mediated apoptosis pathway. (B) The expression of Cleaved-caspase 3 and Cyt C in A549 cells examined by WB assay. A549 cells were incubated with saline, free PTX, free DSF, PTX-DSF physical mixture, NRs, NHRplex and HA-HNRplex. The mass ratio of PTX:DSF is 5:1 and the final concentration of PTX was 10 μg/mL in all preparations. β-Actin was set as the control. Quantification of (C) Cyt C and (D) Cleaved-caspase 3 expressed in preparation-treated A549 cells. (E) The expression of Cleaved-caspase 3 and Cyt C in A549/Taxol cells examined by WB assay. Quantification of (F) Cyt C and (G) Cleaved-caspase 3 in preparation-treated A549/Taxol cells. Data are presented as mean ± SD ($n = 3$). $^{*}P < 0.05$, $^{**}P < 0.01$, $^{\#}P < 0.001$.

by specific receptor-ligand binding between HA and tumor-overexpressed CD44 receptors.

To confirm the tumor targeting, we tested the tissue distribution of free DiR, DiR-HNRplex and DiR-HA-HNRplex by *ex vivo* imaging on harvested heart, liver, spleen, lung, kidney, and tumor tissues after 24 h intravenous post-injection (Fig. 8C). Strong fluorescence intensity of free DiR was observed in liver, spleen and lung. In contrast, barely any fluorescence was detected in tumor tissue. In contrast, for both HNRplex and HA-HNRplex groups, strong fluorescence intensity was observed in the tumor tissues, indicating efficient tumor-targeted delivery and prolonged retention. Simultaneously, quantitative measurement revealed that the fluorescence signal in the HA-HNRplex group tumor tissues was significantly higher than that of the HNRplex group, again substantiating the remarkable tumor-targeting ability of HA-HNRplex (Fig. 8D).

Overall, the results indicated that HA-HNRplex had prolonged half-lives and could effectively target and accumulate in the tumor sites *via* both HA-CD44-mediated combination and nanosize-mediated enhanced permeability and retention (EPR) effect.

3.7. *Anti-MDR tumor therapeutic efficacy*

Formulations including saline, PTX-DSF PM, NRs, HNRplex, and HA-HNRplex were intravenously administrated to A549/Taxol-resistant tumor model mice every 2 days for 5 times. As shown in Fig. 9A, the tumor volume of the saline group increased nearly 12-fold in a 12-day period compared to the initial tumor volume without other treatment, while different extents of tumor growth inhibition were observed in all preparation-treated groups. Detailly, compared to the control group, the PTX-DSF PM, NRs, HNRplex and HA-HNRplex-treated groups represented about 2, 3, 3, and 6-fold decrease in tumor volume, respectively. Furthermore, the image and the weight of tumors harvested from 12-day-treated mice demonstrated consistent results of tumor inhibition rate in each group (Fig. 9B and Supporting Information Fig. S9). The tumor growth inhibition of HNRplex was significantly more significant than PTX-DSF PM ($P < 0.05$) and the NRs ($P < 0.05$) at the end of treatment, indicating the efficient intercellular delivery of Cyt C by NRs and enhanced anti-MDR-tumor effect. Particularly, HA-HNRplex suppressed tumor growth with higher efficacy than HNRplex ($P < 0.05$) at the end of treatment.

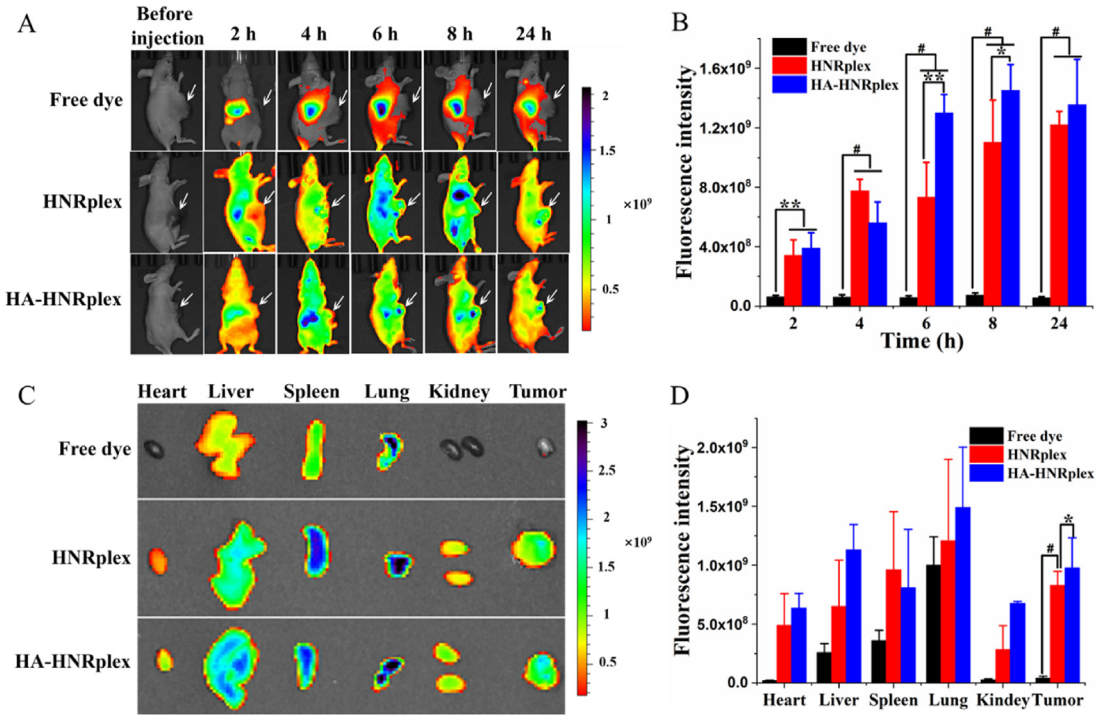

Figure 8 Tumor-targeting *in vivo*. (A) *In vivo* fluorescence imaging in A549/Taxol tumor bearing mice at different time points after i.v. administration of free dye, DiR-labelled NHRplex and HA-HNRplex. The dose of DiR was 1 mg/kg. (B) Semi-quantitative fluorescence intensity analysis of DiR-labeled preparations in tumor. (C) *Ex vivo* fluorescence images of major tissues at 24 h after administration of DiR-labelled HNRplex and HA-HNRplex *via* tail vein. (D) Semi-quantitative data calculated from the fluorescence intensity of DiR-labeled preparations in harvested major organs. Data are presented as mean ± SD ($n = 3$). $^{*}P < 0.05$, $^{**}P < 0.01$, $^{\#}P < 0.001$.

In addition, the alteration in body weight of mice in different groups was recorded during the administration period (Supporting Information Fig. S10). Among them, the body weight of the saline group escalated modestly, while the mice treated with NRs, HNRplex and HA-HNRplex suffered ignored weight loss. However, the body weight of the group treated with PTX-DSF PM showed a significant decrease at the end of treatment, likely due to the solvent polyoxyethylene castor oil and ethanol contained in the formulation and the resultant toxicity.

Finally, we detected histopathological features, proliferation and in situ apoptosis on tumors by H&E staining, Ki67 and TUNEL immunohistochemical staining, respectively. As shown by the H&E staining in Fig. 9C, the tumor cells in the saline group grew densely with more uniform staining of nuclei and cytoplasm, while HA-HNRplex- and HNRplex-treated groups demonstrated large pink areas with reduced cell density and reduced nuclei areas, indicating effective pathological tumor-killing effect. MDR tumors commonly exhibit hyperproliferation and apoptosis resistance, significantly contributing to the failure of treatment[41]. The increased proportion of Ki67-positive cells in tumor tissues is a vital reference indicator to judge hyperproliferation[42]. As suggested by the Ki67 immunohistochemical assay (Fig. 9C and D), the tumors harvested from A549/Taxol tumor-bearing mice displayed the widespread distribution of Ki67-positive cells (brown area), while formulation-treated groups were observed with a reduced rate of hyperproliferative cells. Among these formulations, HA-HNRplex possessed the most profound proliferation inhibition. Additionally, TUNEL immunohistochemical staining was conducted to detect cell apoptosis on tumors (Fig. 9C and E), and the saline-treated group with bare apoptotic cells distributed (green area) was set as the control. Significantly, HA-HNRplex demonstrated more effective cell apoptosis (green area) than other formulations. The results verified that HA-HNRplex is promising to regress hyperproliferation and promote apoptosis on MDR tumors, leading to remarkable anti-MDR-tumor efficiency and considerable biosafety.

3.8. *Mechanism study*

P-gp is a well-known MDR protein and can pump several small-molecule anticancer drugs (*e.g.*, PTX and doxorubicin)[8], whereas DSF is a P-gp inhibitor. As a result, we first detected the P-gp expression on A549 and A549/Taxol cells. As illustrated in Supporting Information Fig. S11, A549/Taxol cells demonstrated a significantly higher expression of P-gp than A549 cells, confirming the drug resistance. The treatment did not affect the protein expression on A549 cells and, in contrast, significantly altered the expression on A549/Taxol cells. The administration of DSF, NRs, HNRplex and HA-HNRplex reduced the expression compared to the saline group (control). We also found that the PTX administration escalated the P-gp level and the treatment of the PTX + DSF cocktail or NRs declined the expression, indicating the rational combination use. Significantly, dosing HA-HNRplex profoundly inhibited the P-gp expression compared to the saline group ($P < 0.01$).

Cyt C activated caspase 3 and promoted apoptosis of tumor cell. As mentioned above, our data indicated that the HA-HNRplex intensified the activation of the caspase 3. Accordingly, we next studied the caspase-pathway role on cell viability and apoptosis, using Q-VD-OpH and Z-VAD-FMK as pan caspase inhibitors[43,44]

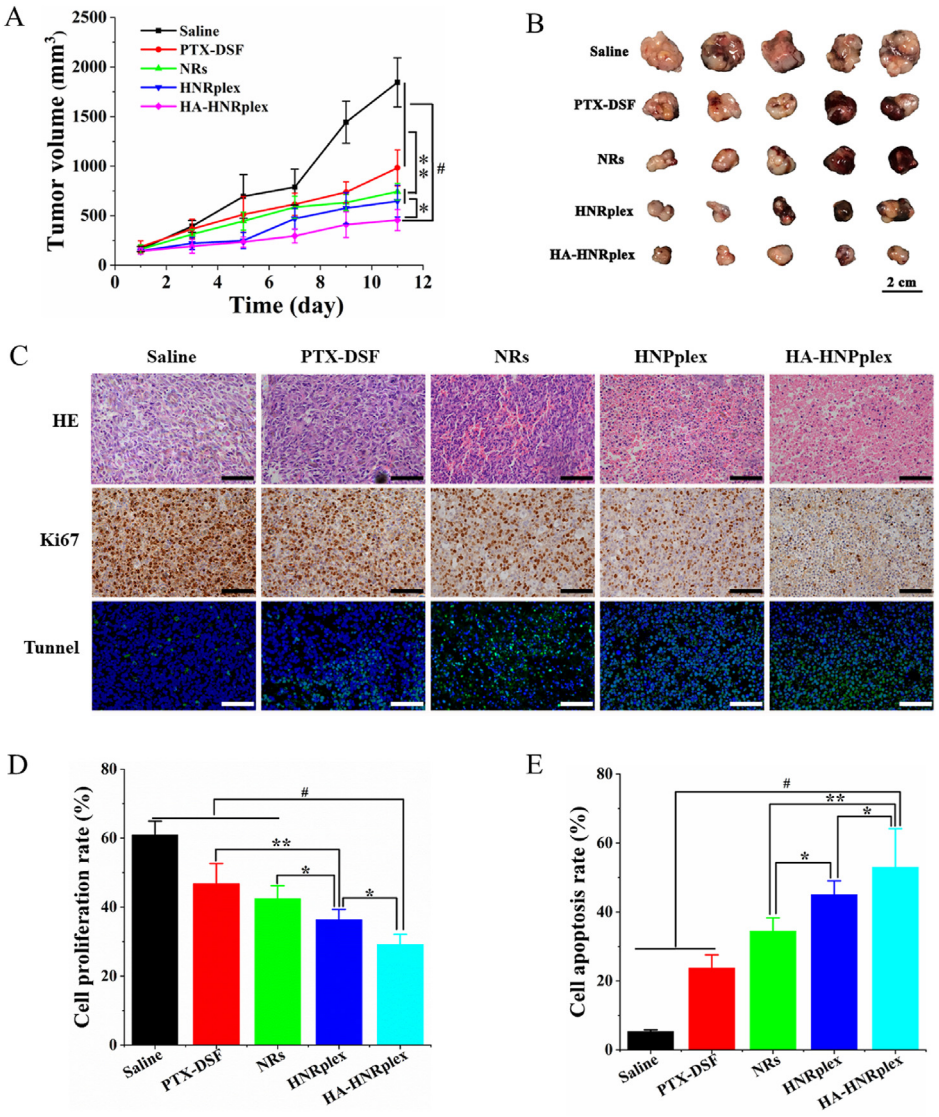

Figure 9 *In vivo* anti-tumor efficiency in A549/Taxol tumor model. (A) Tumor growth curves of A549/Taxol tumor bearing mice treated with different formulations. (B) Digital picture and (C) weight of tumor harvested from A549/Taxol tumor bearing mice after 11-day treatment. (D) H&E staining, Ki67 expression and Tunnel analysis of A549/Taxol tumor tissues after treatment. The scale bar is 50 μm. Semi-quantitative analysis of tumor-cell (E) proliferation and (F) apoptosis calculated *via* Image-Pro Plus software. Data are presented as mean ± SD ($n = 5$), $^{*}P < 0.05$, $^{**}P < 0.01$, $^{\#}P < 0.001$.

and A-DEVD-CHO as a caspase 3 specific inhibitor[45]. As shown in Supporting Information Fig. S12, caspase inhibition by the three inhibitors, especially by the caspase-3-specific blocker (A-DEVD-CHO) compromised the capacity of HA-HNRplex against the cell viability and to induce apoptosis. The caspase-3-specific inhibitor reduced HA-HNRplex's anti-tumor activity with higher efficacy than the other two pan caspase inhibitors, confirming the caspase 3 contribution.

Finally, we detected Cyt C and Cleaved-Caspase 3 protein expression in tumor tissues *via* WB assay after dosing. As indicated in Supporting Information Fig. S13A–S13C, the HA-HNRplex-treated group displayed the highest expression level of Cyt C and Cleaved-Caspase 3 in tumor tissues among all the preparations, increasing by 2-fold and 1.5-fold compared to the control A549/Taxol-resistant tumor model mice, respectively. Increasing evidence has proved that the MDR tumor is characterized by downregulated expression of Cyt C and Cleaved-caspase 3 thereby inhibiting cell apoptosis consistent with our results[46]. Compared to the control group and PTX-DSF PM group, NRs group exhibited higher expression of the two proteins as the cocrystal-based NRs could deliver DSF into tumor cells. HA-HNRplex administration elevated the expression with higher efficacy than NRs and HNRplex, owing to the synergistic effect by relieving MDR *via* DSF and improving the intracellular delivery of Cyt C *via* targeted uptake. The resultant protein expression *in vivo* after treatment is consistent with the cellular experiments (Fig. 7).

Overall, the targeted nanococktail HA-HNRplex combated the MDR-tumor *via* cascade mechanisms by inhibiting P-gp, elevating intercellular Cyt C, upregulating the expression of Cleaved-Caspase 3, and thus, promoting the MDR cell apoptosis.

4. Discussion

Despite enormous advances in chemotherapeutics development, MDR remains a major barrier to effective therapeutic outcomes, posing formidable challenges in clinical cancer treatment[47]. Complicated mechanisms are involved in the formation of MDR tumors; and one of them, the overexpressed P-gp is the most prevalent and studied factor as a typical membrane pump mediating efflux of chemotherapeutics[48]. For drug-resistant tumor cells, single high doses and multiple-repeated doses of chemotherapeutic agents are commonly demanded to reach considerable therapeutic effects, while this strategy is identical to quenching a thirst for poison and the potential to induce the emergence of more drug-resistant phenotype of cancer[49]. Therefore, strategies for combined chemotherapy have received increasing attention for improving anti-tumor outcomes[50]. In our previous study, the combined use of P-gp inhibitor DSF and chemotherapeutic drug PTX exhibited an enhanced inhibitory effect of Taxol-resistant tumor than monotherapy[11]. However, the two-drug therapeutic strategy remained incapable of eradicating tumors; especially, there are still increasing cases in which the two-drug combined clinical schedules lead to malignant outcomes in patients[51]. In this study, we developed a triple-drug nanococktail using the cocrystal@protein-anchoring approach, offering a new approach to co-deliver multiple therapeutic agents. With rod-like morphology and HA modification, HA-HNRplex could specifically bind to the tumor-overexpressed CD44 and improve intercellular delivery of the protein drug *via* caveolar-mediated endocytosis pathway and reduce endolysosome degradation. Accordingly, HA-HNRplex synchronously increased the intercellularly targeted delivery of PTX, DSF and Cyt C, demonstrating effective anti-MDR-tumor effect *via* triple-synergetic mechanisms.

Targeted drug delivery to tumors is a significant challenge for effectively treating MDR melanoma[52,53]. The investigations of pharmacokinetics and biodistribution demonstrated that HA-HNRplex could prolong retention in circulation and remarkably accumulate in the tumor. First, HA coating could decrease the absorption of serum proteins on the nanoparticles and compromise the clearance from the immune system[54]. Moreover, the tumor-targeting of HA-HNRplex was elevated through HA-CD44-mediated specific binding[55,56].

Significantly, the triple-dimensional integrated treatment regimen using HA-HNRplex could effectively treat MDR tumors. The therapeutic enhancement was mainly attributed to cascade manner as follows: (i) extraordinary high drug encapsulation and payload capacity, (ii) prolonged circulation time, (iii) specific dual-targetability (active-passive) to CD44-overexpressed tumor cells, (iv) synergy between PTX, DSF and Cyt C. Compared with the commercial liposomal codelivery product (*e.g.*, Vyxeos®, Daunorubicin and Cytarabine), HA-HNRplex indicated higher drug encapsulation efficiency, more integrated triple antitumor mechanisms, and more effective delivery by non-lysosomal pathways. We substantiated that the triple-codelivery, integrating inhibition of MDR tumor, regression of proliferation and stimulation of cancer cell apoptosis, could significantly suppress the occurrence and development of MDR tumor. Our findings predicted a promising exploration of the combinational application of multiple drugs against MDR tumors using the cocrystal@protein-anchoring platform, providing preliminary evidence for safe and precise clinical oncotherapy.

Finally, we also intensively pondered the perspectives of our current work and raised potential limitations for the platform. We proposed a triple-delivery nanococktail to treat MDR tumor using the cocrystal@protein-anchoring approach. However, further investigations are needed to study the assembly mechanisms of the nanococrystal, *i.e.*, what are the driving forces for the cocrystal formation[57], whether their morphologies are alterable, and if the *in vivo* distribution behaviors can be regulated by designing cocrystal phenotypes, etc. Also, more accurate quantification for *in vivo* pharmacokinetics and biodistribution of each component on HA-HNRplex are needed to modify the drug ratio of formation for more precise therapeutic dosage. Second, MDR tumors are variable in types with complex resistance mechanisms. Hence, our HA-HNRplex nanococktail should be further applied to treat other drug-resistant tumors (*i.e.*, triple-negative breast carcinoma, melanoma, head and neck squamous cell carcinoma, etc.), aiming to prove their clinical potential[58]. Last but not least, our triple-delivery strategy holds the promise of integrating chemotherapeutic molecule/biomacromolecule drugs with other anti-tumor mechanisms to develop novel synergistic anti-MDR-tumor mechanisms for oncotherapy, even predicts enormous potential to broad the application in the treatment of other diseases.

5. Conclusions

In summary, we developed a triple-payload nanococktail platform using a cocrystal@protein-anchoring strategy to treat MDR cancer. We proved that HA-HNRplex allowed targeted triple-payload delivery of MDR inhibitor (DSF), biomacromolecule apoptosis accelerator (Cyt C) with marketed chemotherapeutic drug (PTX) and effective treatment against Taxol-resistant cancer in A549/Taxol tumor-bearing mice, probably acting *via* the cascade mechanisms by P-gp suppression, elevating intercellular Cyt C, upregulating the expression of Cleaved-caspase 3, and promoting the MDR cell apoptosis. Moreover, we found that the NRs could be used as a particle-like carrier to efficiently deliver the basic protein Cyt C into tumor cells through the caveolin/lipid-raft pathway and bypass the endosome/lysosome. Additionally, the active drugs are all clinically used. Crystal-based preparation is simple and controllable, enabling reproducibility and scale-up ability. As a result, the platform has a promising translation perspective.

Acknowledgments

This study was supported by the National Natural Science Foundation of China (Nos. 82073782 and 82241002, China), the Shanghai Science and Technology Committee (No. 19430741500, China), National Key Research and Development Program of China (2018YFA0902000, China), and the Key Laboratory of Modern Chinese Medicine Preparation of Ministry of Education of Jiangxi University of Traditional Chinese Medicine (zdsys-202103, China). We thank Lin Ge of Animal Experimental Center in China Pharmaceutical University for kind help with *in vivo* experiments.

Author contributions

Jiahui Zou and Wei He co-wrote the paper. Xuyang Xing and Jiahui Zou performed the experiments and data collection. All

authors discussed the results and reviewed the manuscript. Xuri Wu, Yuanzhen Xia and Wei He supervised the study. All authors have read and approved the final manuscript.

Conflicts of interest

The authors declare no conflicts of interest.

Appendix A. Supporting information

Supporting information to this article can be found online at https://doi.org/10.1016/j.apsb.2024.08.014.

References

1. Sung H, Ferlay J, Siegel RL, Laversanne M, Soerjomataram I, Jemal A, et al. Global cancer statistics 2020: GLOBOCAN estimates of incidence and mortality worldwide for 36 cancers in 185 countries. *Ca Cancer J Clin* 2021;**71**:209−49.
2. Lin H, Hu BC, He XM, Mao JP, Wang Y, Wang J, et al. Overcoming Taxol-resistance in A549 cells: a comprehensive strategy of targeting P-gp transporter, AKT/ERK pathways, and cytochrome P450 enzyme CYP1B1 by 4-hydroxyemodin. *Biochem Pharmacol* 2020;**171**:113733.
3. Xie YH, Chen YX, Fang JY. Comprehensive review of targeted therapy for colorectal cancer. *Signal Transduct Target Ther* 2020;**5**:22.
4. Liu JJ, Zhu CY, Xu LH, Wang DY, Liu W, Zhang KX, et al. Nano-enabled intracellular calcium bursting for safe and efficient reversal of drug resistance in tumor cells. *Nano Lett* 2020;**20**:8102−11.
5. Higgins CF. Multiple molecular mechanisms for multidrug resistance transporters. *Nature* 2007;**446**:749−57.
6. Patel NR, Pattni BS, Abouzeid AH, Torchilin VP. Nanopreparations to overcome multidrug resistance in cancer. *Adv Drug Deliver Rev* 2013;**65**:1748−62.
7. Eckford PD, Sharom FJ. ABC efflux pump-based resistance to chemotherapy drugs. *Chem Rev* 2009;**109**:2989−3011.
8. Pote MS, Gacche RN. ATP-binding cassette efflux transporters and MDR in cancer. *Drug Discov Today* 2023;**28**:103537.
9. Sofias AM, Dunne M, Storm G, Allen C. The battle of "nano" paclitaxel. *Adv Drug Deliver Rev* 2017;**122**:20−30.
10. Kleczkowska P, Sulejczak D, Zaremba M. Advantages and disadvantages of disulfiram coadministered with popular addictive substances. *Eur J Pharmacol* 2021;**904**:174143.
11. Mohammad IS, Teng C, Chaurasiya B, Yin LF, Wu CY, He W. Drug-delivering-drug approach-based co-delivery of paclitaxel and disulfiram for treating multidrug-resistant cancer. *Int J Pharmaceut* 2019;**557**:304−13.
12. Zhang YJ, Sun T, Jiang C. Biomacromolecules as carriers in drug delivery and tissue engineering. *Acta Pharm Sin B* 2018;**8**:34−50.
13. Santucci R, Sinibaldi F, Cozza P, Polticelli F, Fiorucci L. Cytochrome c: an extreme multifunctional protein with a key role in cell fate. *Int J Biol Macromol* 2019;**136**:1237−46.
14. Hu QY, Sun WJ, Wang C, Gu Z. Recent advances of cocktail chemotherapy by combination drug delivery systems. *Adv Drug Deliver Rev* 2016;**98**:19−34.
15. Lang TQ, Liu YR, Zheng Z, Ran W, Zhai YH, Yin Q, et al. Cocktail strategy based on spatio-temporally controlled nano device improves therapy of breast cancer. *Adv Mater* 2019;**31**:1806202.
16. Yang MY, Zhao RR, Fang YF, Jiang JL, Yuan XT, Shao JW. Carrier-free nanodrug: a novel strategy of cancer diagnosis and synergistic therapy. *Int J Pharmaceut* 2019;**570**:118663.
17. Huang JX, Xiao K. Nanoparticles-based strategies to improve the delivery of therapeutic small interfering RNA in precision oncology. *Pharmaceutics* 2022;**14**:1586.
18. Ghosh S, Javia A, Shetty S, Bardoliwala D, Maiti K, Banerjee S, et al. Triple negative breast cancer and non-small cell lung cancer: clinical challenges and nano-formulation approaches. *J Control Release* 2021;**337**:27−58.
19. Riley RS, June CH, Langer R, Mitchell MJ. Delivery technologies for cancer immunotherapy. *Nat Rev Drug Discov* 2019;**18**:175−96.
20. Xiao QQ, Li XT, Liu C, Jiang YX, He YL, Zhang WT, et al. Improving cancer immunotherapy *via* co-delivering checkpoint blockade and thrombospondin-1 downregulator. *Acta Pharm Sin B* 2023;**13**:3503−17.
21. Zhang J, Hu KL, Di LQ, Wang PL, Liu ZD, Zhang JM, et al. Traditional herbal medicine and nanomedicine: Converging disciplines to improve therapeutic efficacy and human health. *Adv Drug Deliver Rev* 2021;**178**:113964.
22. Magar KT, Boafo GF, Li XT, Chen ZJ, He W. Liposome-based delivery of biological drugs. *Chin Chem Lett* 2022;**33**:587−96.
23. Peng XJ, Li XT, Xie B, Lai YY, Sosnik A, Boucetta H, et al. Gout therapeutics and drug delivery. *J Control Release* 2023;**362**:728−54.
24. Huang L, Zhao SJ, Fang F, Xu T, Lan MH, Zhang JF. Advances and perspectives in carrier-free nanodrugs for cancer chemo-monotherapy and combination therapy. *Biomaterials* 2021;**268**:120557.
25. Iqbal H, Yang T, Li T, Zhang MY, Ke HT, Ding DW, et al. Serum protein-based nanoparticles for cancer diagnosis and treatment. *J Control Release* 2021;**329**:997−1022.
26. Li Y, Teng C, Azevedo HS, Yin LF, He W. Cocrystallization-like strategy for the codelivery of hydrophobic and hydrophilic drugs in a single carrier material formulation. *Chin Chem Lett* 2021;**32**:3071−5.
27. Park JW, Bae KH, Kim C, Park TG. Clustered magnetite nanocrystals cross-linked with PEI for efficient siRNA delivery. *Biomacromolecules* 2011;**12**:457−65.
28. Rong DD, Wang CW, Zhang XM, Wei YL, Zhang ML, Liu DY, et al. A novel taxane, difluorovinyl-ortataxel, effectively overcomes paclitaxel-resistance in breast cancer cells. *Cancer Lett* 2020;**491**:36−49.
29. Li BB, Teng C, Yu HL, Jiang XH, Xing XY, Jiang Q, et al. Alleviating experimental pulmonary hypertension *via* co-delivering FoxO1 stimulus and apoptosis activator to hyperproliferating pulmonary arteries. *Acta Pharm Sin B* 2023;**13**:2369−82.
30. Zhao BL, Su KY, Mao XL, Zhang XW. Separation and identification of enzyme inhibition peptides from dark tea protein. *Bioorg Chem* 2020;**99**:103772.
31. Teng C, Li BB, Lin CS, Xing XY, Huang FF, Yang Y, et al. Targeted delivery of baicalein-p53 complex to smooth muscle cells reverses pulmonary hypertension. *J Control Release* 2022;**341**:591−604.
32. Soleymani M, Velashjerdi M, Shaterabadi Z, Barati A. One-pot preparation of hyaluronic acid-coated iron oxide nanoparticles for magnetic hyperthermia therapy and targeting CD44-overexpressing cancer cells. *Carbohyd Polym* 2020;**237**:116130.
33. Patel V, Rajani C, Tambe V, Kalyane D, Anup N, Deb PK, et al. Nanomaterials assisted chemo-photothermal therapy for combating cancer drug resistance. *J Drug Deliv Sci Tec* 2022;**70**:103164.
34. Duan C, Yu M, Xu J, Li BY, Zhao Y, Kankala RK. Overcoming cancer multidrug resistance (MDR): reasons, mechanisms, nanotherapeutic solutions, and challenges. *Biomed Pharmacother* 2023;**162**:114643.
35. Zhang ZL, Xia T, Ran P, Wei JW, Meng J, Zhang GY, et al. Persistent luminescence-activated Janus nanomotors with integration of photodynamic and photothermal cancer therapies. *Chem Eng J* 2023;**457**:141226.
36. Du XQ, Hou YQ, Huang J, Pang Y, Ruan CL, Wu W, et al. Cytosolic delivery of the immunological adjuvant Poly I:C and cytotoxic drug crystals *via* a carrier-free strategy significantly amplifies immune response. *Acta Pharm Sin B* 2021;**11**:3272−85.
37. Machtakova M, ThérienAubin H, Landfester K. Polymer nanosystems for the encapsulation and delivery of active biomacromolecular therapeutic agents. *Chem Soc Rev* 2022;**51**:128−52.
38. Asrorov AM, Gu ZY, Li F, Liu LY, Huang YZ. Biomimetic camouflage delivery strategies for cancer therapy. *Nanoscale* 2021;**13**:8693−706.

39. Mnich K, Carleton LA, Kavanagh ET, Doyle KM, Samali A, Gorman AM. Nerve growth factor-mediated inhibition of apoptosis post-caspase activation is due to removal of active caspase-3 in a lysosome-dependent manner. *Cell Death Dis* 2014;**5**:e1202.
40. Bae YH, Park K. Targeted drug delivery to tumors: myths, reality and possibility. *J Control Release* 2011;**153**:198−205.
41. Assaraf YG, Brozovic A, Gonçalves AC, Jurkovicova D, Linē A, Machuqueiro M, et al. The multi-factorial nature of clinical multidrug resistance in cancer. *Drug Resist Update* 2019;**46**:100645.
42. Zhao XH, Liu YM, Li ZH, Zheng SY, Wang ZR, Li WZ, et al. Linc00511 acts as a competing endogenous RNA to regulate VEGFA expression through sponging hsa-miR-29b-3p in pancreatic ductal adenocarcinoma. *J Cel Mol Med* 2018;**22**:655−67.
43. Keoni CL, Brown TL. Inhibition of apoptosis and efficacy of pan caspase inhibitor, Q-VD-OPh, in models of human disease. *J Cel Death* 2015;**8**. JCD. S23844.
44. Clark P, Dziarmaga A, Eccles M, Goodyer P. Rescue of defective branching nephrogenesis in renal-coloboma syndrome by the caspase inhibitor, Z-VAD-fmk. *J Am Soc Nephrol* 2004;**15**:299−305.
45. Zhang CC, Li CG, Wang YF, Xu LH, He XH, Zeng QZ, et al. Chemotherapeutic paclitaxel and cisplatin differentially induce pyroptosis in A549 lung cancer cells *via* caspase-3/GSDME activation. *Apoptosis* 2019;**24**:312−25.
46. Zhang TT, Liu H, Liu M, Wang CH. Farrerol suppresses the progression of laryngeal squamous cell carcinoma *via* the mitochondria-mediated pathway. *Eur J Pharmacol* 2021;**913**:174636.
47. Dallavalle S, Dobričić V, Lazzarato L, Gazzano E, Machuqueiro M, Pajeva I, et al. Improvement of conventional anticancer drugs as new tools against multidrug resistant tumors. *Drug Resist Update* 2020;**50**:100682.
48. Lee T, Kim KS, Na K. Nanocracker capable of simultaneously reversing both P-glycoprotein and tumor microenvironment. *J Control Release* 2023;**354**:268−78.
49. Liu JB, Song LL, Liu SL, Zhao S, Jiang Q, Ding BQ. A tailored DNA nanoplatform for synergistic RNAi-/chemotherapy of multidrug-resistant tumors. *Angew Chem Int Edit* 2018;**57**:15486−90.
50. Liu SG, Khan AR, Yang XY, Dong B, Ji JB, Zhai G. The reversal of chemotherapy-induced multidrug resistance by nanomedicine for cancer therapy. *J Control Release* 2021;**335**:1−20.
51. West JB, Dinh MN, Brown JS, Zhang J, Anderson AR, Gatenby RA. Multidrug cancer therapy in metastatic castrate-resistant prostate cancer: an evolution-based strategy. *Clin Cancer Res* 2019;**25**:4413−21.
52. Roy A, Ernsting MJ, Undzys E, Li SD. A highly tumor-targeted nanoparticle of podophyllotoxin penetrated tumor core and regressed multidrug resistant tumors. *Biomaterials* 2015;**52**:335−46.
53. Lepeltier E, Rijo P, Rizzolio F, Popovtzer R, Petrikaite V, Assaraf YG, et al. Nanomedicine to target multidrug resistant tumors. *Drug Resist Update* 2020;**52**:100704.
54. Kang Y, Sun W, Li SY, Li ML, Fan JL, Du JJ, et al. Oligo hyaluronan-coated silica/hydroxyapatite degradable nanoparticles for targeted cancer treatment. *Adv Sci* 2019;**6**:1900716.
55. Meng J, Jin ZK, Zhao PH, Zhao B, Fan MJ, He QJ. A multistage assembly/disassembly strategy for tumor-targeted CO delivery. *Sci Adv* 2020;**6**:eaba1362.
56. Boafo GF, Shi YJ, Xiao QQ, Magar KT, Zoulikha M, Xing XY, et al. Targeted co-delivery of daunorubicin and cytarabine based on the hyaluronic acid prodrug modified liposomes. *Chin Chem Lett* 2022;**33**:4600−4.
57. Springuel Gr, Norberg B, Robeyns K, Wouters J, Leyssens T. Advances in pharmaceutical cocrystal screening: effective cocrystal screening through structural resemblance. *Cryst Growth Des* 2012;**12**:475−84.
58. Robey RW, Pluchino KM, Hall MD, Fojo AT, Bates SE, Gottesman MM. Revisiting the role of ABC transporters in multidrug-resistant cancer. *Nat Rev Cancer* 2018;**18**:452−64.